

# Determination of the $\Delta(1232)$ axial and pseudoscalar form factors from lattice QCD

Constantia Alexandrou

*Department of Physics, University of Cyprus, P.O. Box 20537, 1678 Nicosia, and  
The Cyprus Institute, P.O. Box 27546, 1645 Nicosia, Cyprus*

Eric B. Gregory

*Bergische Universität Wuppertal, Gaussstr. 20, D-42119 Wuppertal, Germany*

Tomasz Korzec

*Institut für Physik, Humboldt Universität zu Berlin, Newtonstrasse 15, 12489 Berlin, Germany*

Giannis Koutsou

*Cyprus Institute, CaSToRC, 20 Kavafi Street, Nicosia 2121, Cyprus*

John Negele

*Center for Theoretical Physics, Laboratory for Nuclear Science and Department of Physics,  
Massachusetts Institute of Technology, Cambridge, Massachusetts 02139, U.S.A.*

Toru Sato

*Department of Physics, Osaka University, Osaka 560-0043, Japan*

Antonios Tsapalis

*Hellenic Naval Academy, Hatzikyriakou Ave., Pireaus 18539, Greece and  
Department of Physics, National Technical University of Athens, Zografou Campus 15780, Athens, Greece  
(Dated: February 27, 2024)*

We present a lattice QCD calculation of the  $\Delta(1232)$  matrix elements of the axial-vector and pseudoscalar currents. The decomposition of these matrix elements into the appropriate Lorentz invariant form factors is carried out and the techniques to calculate the form factors are developed and tested using quenched configurations. Results are obtained for  $2 + 1$  domain wall fermions and within a hybrid scheme with domain wall valence and staggered sea quarks. Two Goldberger-Treiman type relations connecting the axial to the pseudoscalar effective couplings are derived. These and further relations based on the pion-pole dominance hypothesis are examined using the lattice QCD results, finding support for their validity. Utilizing lattice QCD results on the axial charges of the nucleon and the  $\Delta$ , as well as the nucleon-to- $\Delta$  transition coupling constant, we perform a combined chiral fit to all three quantities and study their pion mass dependence as the chiral limit is approached.

PACS numbers:

## I. INTRODUCTION

Great progress has been made in lattice QCD studies of hadron spectroscopy and structure and lattice QCD results are beginning to provide input to phenomenology and experiment. Simulations with dynamical quarks near and at the physical pion mass [1–4] have been shown to produce the observed low-lying hadron spectrum [2, 5, 6] and  $\pi^+ - \pi^+$  scattering lengths have been calculated to good accuracy [7–10].

Whereas producing experimentally measured quantities from first principles provides a powerful validation of the lattice QCD methodology, calculating quantities that are difficult to extract or have impact in probing physics beyond the standard model is a much more challenging prospective. Studying the structure of the  $\Delta$  resonance is an example of the input lattice QCD can provide to phenomenology that cannot be directly extracted from experiments. This is because the  $\Delta$  decays strongly with a lifetime of  $\sim 10^{-23}$  seconds [11, 12] and resists experimental probing. Measurements of the  $\Delta^+$  magnetic moment exist albeit with a large experimental uncertainty. The  $\Delta$ , having width  $\Gamma \sim 118$  MeV and lying close to the  $\pi N$  threshold, plays an important role in chiral expansions. In heavy baryon chiral perturbation theory it has been included as an explicit degree of freedom [13–16], where it is argued that it improves chiral expansions applied in the description of lattice QCD results such as the nucleon axial charge [36]. Chiral langragians with  $\Delta$  degrees of freedom involve additional coupling constants that are difficult to measure. Therefore, one either treats them as free parameters to be fitted along other parameters using lattice QCD results [13, 17] and data extracted from partial-wave analysis of scattering measurements [15, 16] or estimates them based on phenomenology

and symmetries. For example, one can relate the nucleon axial charge  $g_A$ , which is well measured, to the  $\Delta$  axial charge, in the large- $N_c$  limit [18] or using  $SU(4)$  symmetry [19]. The Goldberger-Treiman (GT) relation is then used to get the effective  $\pi\Delta\Delta$  coupling. Another framework to extract the  $\pi\Delta\Delta$  coupling is via sum rules [20].

Lattice QCD provides a nice framework to study the  $\Delta$  properties and calculate the  $\Delta$  coupling constants. In some of our recent work we developed the formalism to study the  $N - \Delta$  transition form-factors within lattice QCD [21, 22], as well as the  $\Delta$  electromagnetic form-factors [23]. The quadrupole electromagnetic form factor, extracted for the first time, provided input for the deformation of the  $\Delta$  showing that in the infinite momentum frame the  $\Delta$  is prolate [24].

In this work, we present a detailed study of the axial-vector and pseudoscalar form factors of the  $\Delta$ . The theoretical framework and a subset of the results were given in Ref. [25]. Here we discuss in detail the lattice techniques developed and utilized for the extraction of these form factors. In addition, we present an extended analysis of the momentum dependence of all the form factors using an additional ensemble of dynamical domain wall fermions. We also include a study of the pion-pole dominance predictions and compare them to our lattice QCD results.

The outline of the paper is as follows: In Section II we present the decomposition of the  $\Delta$  matrix elements of the axial-vector and pseudoscalar currents. In Section III we explain our lattice techniques and discuss the ensembles utilized for the calculation. In Section IV we present the lattice results on all form factors and examine several relations among them and their phenomenological consequences. In Section V we perform a combined chiral fit using our results on the nucleon axial charge  $g_A$  [26], the  $\Delta$  axial charge  $G_{\Delta\Delta}$  calculated in this work and the dominant axial  $N - \Delta$  transition form factor,  $C_5^A$ , calculated in previous work on the same sets of lattices [22]. Finally, in Section VI we give a summary and conclusions. Technical details and our values on the form factors are presented in the Appendices.

## II. THE AXIAL AND PSEUDOSCALAR MATRIX ELEMENT OF THE $\Delta$

Lorentz invariance and spin-parity rules determine the decomposition of the  $\Delta^+$  matrix element of the isovector axial-vector current in terms of four invariant functions of the momentum transfer squared,  $q^2 = (p_f - p_i)^2$ :

$$\begin{aligned} \langle \Delta^+(p_f, s_f) | A^\mu(0) | \Delta^+(p_i, s_i) \rangle &= \bar{u}_\sigma^\Delta(p_f, s_f) [\mathcal{O}^{\mu A}]^{\sigma\tau} u_\tau^\Delta(p_i, s_i) \\ [\mathcal{O}^{\mu A}]^{\sigma\tau} &= -\frac{1}{2} \left[ g^{\sigma\tau} \left( g_1(q^2) \gamma^\mu \gamma^5 + g_3(q^2) \frac{q^\mu}{2M_\Delta} \gamma^5 \right) + \frac{q^\sigma q^\tau}{4M_\Delta^2} \left( h_1(q^2) \gamma^\mu \gamma^5 + h_3(q^2) \frac{q^\mu}{2M_\Delta} \gamma^5 \right) \right], \end{aligned} \quad (1)$$

where  $p_i(s_i)$  denotes the initial momentum (spin) of the  $\Delta$  and  $p_f(s_f)$  the final momentum (spin). The flavor-isovector axial-vector current operator is defined as

$$A^\mu(x) = \bar{\psi}(x) \gamma^\mu \gamma_5 \frac{\tau^3}{2} \psi(x) \quad (2)$$

where  $\tau^3$  denotes the Pauli matrix acting in flavor space and  $\psi(x)$  is the isospin quark doublet. The four axial form factors,  $g_1, g_3, h_1$  and  $h_3$  as defined in Eq. (1) are grouped into the familiar structure of the nucleon axial-vector vertex.

In the description of spin-3/2 energy-momentum eigenstates, classical solutions of the Rarita-Schwinger equation play a central role. Each component of a vector-spinor  $u_\sigma$ , with  $\sigma$  a Lorentz four-vector index solves the free Dirac equation

$$[\not{p} - M_\Delta] u_\sigma^\Delta(p, s) = 0. \quad (3)$$

Implementing additionally the constraint equations,

$$p^\sigma u_\sigma^\Delta(p, s) = 0 \quad \text{and} \quad \gamma^\sigma u_\sigma^\Delta(p, s) = 0, \quad (4)$$

the unphysical components are eliminated and the remaining eight degrees of freedom describe a spin-3/2 (anti-)particle. Rarita-Schwinger spinors satisfy the spin sum relation:

$$\begin{aligned} \Lambda_{\sigma\tau} &\equiv \sum_{s=-3/2}^{3/2} u_\sigma^\Delta(p, s) \bar{u}_\tau^\Delta(p, s) \\ &= -\frac{\not{p} + M_\Delta}{2M_\Delta} \left( g_{\sigma\tau} - \frac{\gamma_\sigma \gamma_\tau}{3} - \frac{2p_\sigma p_\tau}{3M_\Delta^2} + \frac{p_\sigma \gamma_\tau - p_\tau \gamma_\sigma}{3M_\Delta} \right), \end{aligned} \quad (5)$$

where the normalization  $\bar{u}^{\Delta\sigma} u_{\sigma}^{\Delta} = -1$  is assumed.

The zero momentum transfer limit of (1) defines the axial charge,  $G_{\Delta\Delta}$  of the  $\Delta$  multiplet. Ref [27] normalizes the axial charge via

$$\langle \Delta^{++} | A_{\mu}^3 | \Delta^{++} \rangle - \langle \Delta^{-} | A_{\mu}^3 | \Delta^{-} \rangle = G_{\Delta\Delta} \mathcal{M}_{\mu} \quad (6)$$

where  $\mathcal{M}_{\mu}$  encodes the spin structure of the forward matrix element

$$\mathcal{M}_{\mu} = \bar{u}^{\Delta\sigma}(p) \gamma_{\mu} \gamma_5 u_{\sigma}^{\Delta}(p) . \quad (7)$$

Following the above normalization we establish via Eq. (1):

$$G_{\Delta\Delta} = -3g_1(0) . \quad (8)$$

We note that while the Lorentz decomposition of the axial current is naturally expressed via  $g_1, g_3, h_1$  and  $h_3$  as in Eq.(1), a decomposition in terms of multipoles is possible as for example in the case of the  $\Delta$  electromagnetic transition [23]. Such a representation is more easily expressed in the Breit frame. This decomposition is performed in Appendix A in terms of four multipoles,  $L_1, L_3, E_1$  and  $E_3$ , and their relation to the form factors  $g_1, g_3, h_1$  and  $h_3$  is given.

The  $\Delta^+$  matrix element of the pseudoscalar density operator

$$P(x) = \bar{\psi}(x) \gamma_5 \frac{\tau^3}{2} \psi(x) \quad (9)$$

is decomposed in terms of two Lorentz invariant form factors, denoted by  $\tilde{g}(q^2)$  and  $\tilde{h}(q^2)$ :

$$\begin{aligned} \langle \Delta^+(p_f, s_f) | P(0) | \Delta^+(p_i, s_i) \rangle &= \bar{u}_{\sigma}^{\Delta}(p_f, s_f) [\mathcal{O}^P]^{\sigma\tau} u_{\tau}^{\Delta}(p_i, s_i), \\ [\mathcal{O}^{PS}]^{\sigma\tau} &= -\frac{1}{2} \left[ g^{\sigma\tau} (\tilde{g}\gamma^5) + \frac{q^{\sigma} q^{\tau}}{4M_{\Delta}^2} (\tilde{h}\gamma^5) \right] . \end{aligned} \quad (10)$$

While  $\tilde{g}(q^2)$  and  $\tilde{h}(q^2)$  are the directly computable form factors from the three-point pseudoscalar correlator, they can be related to the phenomenologically more interesting pion- $\Delta$  vertex using the partially conserved axial current hypothesis (PCAC). Using PCAC on the hadronic level one can write

$$\partial^{\mu} A_{\mu}^a = f_{\pi} m_{\pi}^2 \pi^a , \quad (11)$$

with  $\pi^a$  denoting the isotriplet pion field operator. In the SU(2) symmetric limit of QCD with  $m_q$  denoting the up/down mass, the pseudo-scalar density is related to the divergence of the axial-vector current through the axial Ward-Takahashi identity (AWI)

$$\partial^{\mu} A_{\mu}^a = 2m_q P^a = f_{\pi} m_{\pi}^2 \pi^a , \quad (12)$$

with operators now defined as quark bilinears. Using the relations of Eqs. (11) and (12) we identify the physically relevant pion- $\Delta$ - $\Delta$  form factor  $G_{\pi\Delta\Delta}(q^2)$ , which at  $q^2 = 0$  gives the  $\pi\Delta\Delta$  coupling, as well as a second form factor  $H_{\pi\Delta\Delta}(q^2)$ , by rewriting the pseudoscalar matrix element as

$$2m_q \langle \Delta^+(p_f, s_f) | P(0) | \Delta^+(p_i, s_i) \rangle \equiv \frac{f_{\pi} m_{\pi}^2}{(q^2 - m_{\pi}^2)} \times \bar{u}_{\sigma}^{\Delta} \left[ g^{\sigma\tau} G_{\pi\Delta\Delta}(q^2) + \frac{q^{\sigma} q^{\tau}}{4M_{\Delta}^2} H_{\pi\Delta\Delta}(q^2) \right] \gamma^5 u_{\tau}^{\Delta} , \quad (13)$$

where we effectively make the identification

$$G_{\pi\Delta\Delta}(q^2) \equiv \frac{m_q(m_{\pi}^2 - q^2)}{f_{\pi} m_{\pi}^2} \tilde{g}(q^2) \quad (14)$$

$$H_{\pi\Delta\Delta}(q^2) \equiv \frac{m_q(m_{\pi}^2 - q^2)}{f_{\pi} m_{\pi}^2} \tilde{h}(q^2) . \quad (15)$$

At zero momentum transfer  $q^2 = 0$  only  $G_{\pi\Delta\Delta}$  can be extracted. This coupling is analogous to the known  $\pi - N$  pseudoscalar coupling constant  $G_{\pi NN}$  defined for the nucleon. For the discussion presented in the next section it is

useful to recall the definition of the corresponding quantities in the nucleon sector [21]. For the matrix elements of the axial-vector current we have

$$\langle N(p_f, s_f) | A_\mu^3 | N(p_i, s_i) \rangle = i \frac{1}{2} \bar{u}_N \left[ G_A(q^2) \gamma_\mu \gamma_5 + \frac{q_\mu \gamma_5}{2m_N} G_P(q^2) \right] u_N \quad (16)$$

and for the pseudoscalar density

$$2m_q \langle N(p_f, s_f) | P^3 | N(p_i, s_i) \rangle = \frac{f_\pi m_\pi^2}{(q^2 - m_\pi^2)} \times \bar{u}_N [G_{\pi NN}(q^2)] i \gamma^5 u_N. \quad (17)$$

Note that we have dropped for simplicity an overall kinematical factor arising from the normalization of lattice states, since it is of no relevance for our discussion here.

### A. Goldberger-Treiman Relations

In this section we apply PCAC to derive GT relations for the  $\Delta$ . We recall that PCAC has been shown to apply satisfactorily in the nucleon case leading to the Goldberger-Treiman (GT) relation. This can be derived from Eqs. (16) and (17) related by AWI and taking  $q^2 = 0$  to obtain  $G_{\pi NN}$  in terms of the nucleon axial charge via the relation

$$f_\pi G_{\pi NN}(0) = m_N G_A(0). \quad (18)$$

Assuming  $G_{\pi NN}$  varies smoothly with  $q^2$  so that  $G_{\pi NN}(0) \sim G_{\pi NN}(m_\pi^2) \equiv g_{\pi NN}$  then the GT relates the physical coupling constant  $g_{\pi NN}$  with the nucleon axial charge  $g_A$ . At the chiral limit, using  $\partial_\mu A_\mu = 0$  one derives that  $G_P(q^2) = -\frac{4m_N^2}{q^2} G_A(q^2)$ . Therefore,  $g_{\pi NN}$  measures the chiral symmetry breaking. PCAC dictates that the form factor  $G_P(q^2)$  has a pion pole given by  $G_P(q^2) = \frac{4m_N f_\pi}{m_\pi^2 - q^2} G_{\pi NN}(q^2)$ . The validity of the GT relation and the momentum dependence of  $G_P(q^2)$  in the nucleon case has been studied in Ref. [21]. Similarly, a non-diagonal GT relation, applicable to the axial  $N$ -to- $\Delta$  transition is formulated and relates the axial  $N\Delta$  coupling  $c_A$  to the  $\pi N\Delta$  effective coupling. Lattice calculations examined the validity of the non-diagonal GT relation using the same ensembles as in this work [22].

One can similarly derive GT relations for the  $\Delta$  by taking the matrix elements of the AWI with  $\Delta$  states,  $\langle \Delta | \partial_\mu A^\mu | \Delta \rangle = 2m_q \langle \Delta | P | \Delta \rangle$ . Taking the dot-product of  $q_\mu$  with the matrix element of the axial-vector current given in Eq. (1) we obtain

$$m_\Delta \left[ g^{\sigma\tau} (g_1 - \tau g_3) + \frac{q^\sigma q^\tau}{4M_\Delta^2} (h_1 - \tau h_3) \right] = \frac{f_\pi m_\pi^2}{(m_\pi^2 - q^2)} \left[ g^{\sigma\tau} G_{\pi\Delta\Delta} + \frac{q^\sigma q^\tau}{4M_\Delta^2} H_{\pi\Delta\Delta} \right], \quad (19)$$

where  $\tau = -q^2/(2M_\Delta)^2$ . By considering  $\sigma \neq \tau$  in Eq. (19) we derive the relation

$$m_\Delta (h_1 - \tau h_3) = \frac{f_\pi m_\pi^2 H_{\pi\Delta\Delta}(q^2)}{m_\pi^2 - q^2}, \quad (20)$$

which implies that

$$M_\Delta (g_1 - \tau g_3) = \frac{f_\pi m_\pi^2 G_{\pi\Delta\Delta}(q^2)}{m_\pi^2 - q^2}. \quad (21)$$

One possible linear combination of Eqs. (20) and (21) can be obtained by taking the dot product of Eq. (19) with  $q_\tau$  leading to

$$M_\Delta [(g_1 - \tau g_3) - \tau (h_1 - \tau h_3)] = \frac{f_\pi m_\pi^2}{m_\pi^2 - q^2} [G_{\pi\Delta\Delta} - \tau H_{\pi\Delta\Delta}], \quad (22)$$

which can be considered as a generalized GT-type relation connecting all the six form factors. At  $q^2 = 0$  and assuming all terms in Eq. (22) are finite we obtain

$$f_\pi G_{\pi\Delta\Delta}(0) = m_\Delta g_1(0). \quad (23)$$

If  $G_{\pi\Delta\Delta}$  is a continuous slow varying function of  $q^2$  as  $q^2 \rightarrow 0$  then  $G_{\pi\Delta\Delta}(m_\pi^2) \sim G_{\pi\Delta\Delta}(0)$  and we thus derive a GT relation for the  $\Delta$  analogous to the one for the nucleon case.

Using Eq. 20 and setting  $q^2 = 0$  we obtain a second GT relation

$$f_\pi H_{\pi\Delta\Delta}(0) = m_\Delta h_1(0). \quad (24)$$

If one invokes pion-pole dominance and noting that  $g_1$  and  $G_{\pi\Delta\Delta}$  are both finite at the origin, it follows from Eqs. (21, 20) that as  $q^2 \rightarrow m_\pi^2$   $g_3$  and  $h_3$  must have a pole at  $q^2 = m_\pi^2$ . We thus arrive at the relations

$$g_1 = \frac{f_\pi}{M_\Delta} G_{\pi\Delta\Delta} \quad , \quad g_3 = \frac{4f_\pi M_\Delta}{m_\pi^2 - q^2} G_{\pi\Delta\Delta} . \quad (25)$$

and

$$h_1 = \frac{f_\pi}{M_\Delta} H_{\pi\Delta\Delta} \quad , \quad h_3 = \frac{4f_\pi M_\Delta}{m_\pi^2 - q^2} H_{\pi\Delta\Delta} . \quad (26)$$

It is thus interesting to note how the spin-3/2 nature of the  $\Delta$  state combined with PCAC leads to a *pair* of Goldberger-Treiman relations, given by Eqs. (23) and (24). Let us examine further these relations at the chiral limit. From Eq. (22) we find that

$$h_1 - \tau h_3 = \frac{g_1 - \tau g_3}{\tau}, \quad (27)$$

which means that in the limit  $q^2 \rightarrow 0$  the leadin behavior of  $h_1 \sim 1/q^2$ ,  $h_3 \sim 1/(q^2)^2$  via Eq. (20) and  $H_{\pi\Delta\Delta} \sim 1/q^2$  via Eq. (26). Therefore, the second GT-type relation given in Eq. (24) cannot be extrapolated to physical pion mass since the assumption that  $h_1$  and  $H_{\pi\Delta\Delta}$  are slowly varying functions of  $q^2$  no longer holds. However, since they both display a pion-pole behaviour one can factor it out on both sides and thus the ratio  $h_1/H_{\pi\Delta\Delta}$  can be extrapolated to the physical pion. In this sense, this constitutes a second GT relation.

### III. LATTICE EVALUATION

#### A. Euclidean Correlators and Form Factors

Standard techniques are employed on the Euclidean space-time lattice for the evaluation of hadronic form factors. The following two-point and three-point functions are required:

$$\begin{aligned} G_{\sigma\tau}(\Gamma^\nu, \vec{p}, t_f) &= \sum_{\vec{x}_f} e^{-i\vec{x}_f \cdot \vec{p}} \Gamma_{\alpha'\alpha}^\nu \langle \chi_{\sigma\alpha}(t_f, \vec{x}_f) \bar{\chi}_{\tau\alpha'}(0, \vec{0}) \rangle \\ G_{\sigma\mu\tau}^A(\Gamma^\nu, \vec{q}, t; t_f) &= \sum_{\vec{x}, \vec{x}_f} e^{+i\vec{x} \cdot \vec{q}} \Gamma_{\alpha'\alpha}^\nu \langle \chi_{\sigma\alpha}(t_f, \vec{x}_f) A_\mu(t, \vec{x}) \bar{\chi}_{\tau\alpha'}(0, \vec{0}) \rangle \\ G_{\sigma\tau}^{\text{PS}}(\Gamma^\nu, \vec{q}, t; t_f) &= \sum_{\vec{x}, \vec{x}_f} e^{+i\vec{x} \cdot \vec{q}} \Gamma_{\alpha'\alpha}^\nu \langle \chi_{\sigma\alpha}(t_f, \vec{x}_f) P(t, \vec{x}) \bar{\chi}_{\tau\alpha'}(0, \vec{0}) \rangle, \end{aligned} \quad (28)$$

where  $P(t, \vec{x})$  and  $A_\mu(t, \vec{x})$  are the lattice pseudoscalar or axial current insertions, and  $\chi$  is the standard lattice interpolating field with overlap with the  $\Delta^+$  quantum numbers:

$$\chi_{\sigma\alpha}^{\Delta^+}(x) = \frac{1}{\sqrt{3}} \epsilon^{abc} \left[ 2 (\mathbf{u}^{a\top}(x) C \gamma_\sigma \mathbf{d}^b(x)) \mathbf{u}_\alpha^c(x) + (\mathbf{u}^{a\top}(x) C \gamma_\sigma \mathbf{u}^b(x)) \mathbf{d}_\alpha^c(x) \right]. \quad (29)$$

The overlap of  $\chi$  with the spin-3/2  $\Delta^+$  is

$$\langle \Omega | \chi_{\sigma\alpha}(0) | \Delta(p, s) \rangle = Z u_{\sigma\alpha}^\Delta(p, s), \quad \langle \Delta(p, s) | \bar{\chi}_{\sigma\alpha}(0) | \Omega \rangle = Z^* \bar{u}_{\sigma\alpha}^\Delta(p, s). \quad (30)$$

We will use the following  $\Gamma$  matrices, which project onto positive parity for zero momentum, for our calculation

$$\Gamma^4 = \frac{1}{4}(\mathbf{1} + \gamma^4), \quad \Gamma^k = \frac{i}{4}(\mathbf{1} + \gamma^4) \gamma_5 \gamma_k, \quad k = 1, 2, 3. \quad (31)$$

The Fourier transforms in (28) enforce a static  $\Delta$  sink at the timeslice  $t_f$  and a momentum transfer  $\vec{q} = -\vec{p}$  injected via the operator insertion at an intermediate timeslice  $t$ .

We insert into these correlators complete sets of hadronic energy momentum eigenstates:

$$\sum_{n,p,\xi} \frac{M_n}{VE_{n(p)}} |n(p,\xi)\rangle \langle n(p,\xi)| = \mathbf{1}, \quad (32)$$

where with  $\xi$  we denote collectively all quantum numbers including spin. For large Euclidean time separations  $t$  and  $t_f - t$  the ground state propagation dominates the correlator:

$$\begin{aligned} G_{\sigma\tau}(\Gamma^\nu, \vec{p}, t) &= \frac{M_\Delta}{E_{\Delta(p)}} |Z|^2 e^{-E_{\Delta(p)}t} \text{tr} [\Gamma^\nu \Lambda_{\sigma\tau}^E(p)] + \text{excited states} \\ G_{\sigma\mu\tau}^A(\Gamma^\nu, \vec{q}, t; t_f) &= \frac{M_\Delta}{E_{\Delta(p)}} |Z|^2 e^{-M_\Delta(t_f-t)} e^{-E_{\Delta(p)}t} \text{tr} [\Gamma^\nu \Lambda_{\sigma\sigma'}^E(0) \mathcal{O}_{\sigma'\mu\tau'}^{E,A} \Lambda_{\tau'\tau}^E(p)] \\ &\quad + \text{excited states} \\ G_{\sigma\tau}^{\text{PS}}(\Gamma^\nu, \vec{q}, t; t_f) &= \frac{M_\Delta}{E_{\Delta(p)}} |Z|^2 e^{-M_\Delta(t_f-t)} e^{-E_{\Delta(p)}t} \text{tr} [\Gamma^\nu \Lambda_{\sigma\sigma'}^E(0) \mathcal{O}_{\sigma'\tau'}^{E,PS} \Lambda_{\tau'\tau}^E(p)] \\ &\quad + \text{excited states} \end{aligned} \quad (33)$$

The Wick-rotated axial and pseudoscalar operators take the form

$$\mathcal{O}_{\sigma\mu\tau}^{E,A} = \frac{1}{2} \left[ \delta_{\sigma\tau} \left( g_1(Q^2) \gamma_\mu \gamma_5 - i \frac{g_3(Q^2)}{2M_\Delta} Q_\mu \gamma_5 \right) - \frac{Q_\sigma^E Q_\tau^E}{(2M_\Delta)^2} \left( h_1(Q^2) \gamma_\mu \gamma_5 - i \frac{h_3(Q^2)}{2M_\Delta} Q_\mu \gamma_5 \right) \right], \quad (34)$$

$$\mathcal{O}_{\sigma\tau}^{E,PS} = \frac{1}{2} \left[ \delta_{\sigma\tau} (\tilde{g}(Q^2) \gamma_5) - \frac{Q_\sigma Q_\tau}{(2M_\Delta)^2} (\tilde{h}(Q^2) \gamma_5) \right], \quad (35)$$

with the Euclidean four-momentum transfer  $Q_\mu = (i(M_\Delta - E_{\Delta(p)}), -\vec{q})$ . The Rarita-Schwinger spin-sum relation becomes

$$\Lambda_{\sigma\tau}^E = -\frac{i\not{p} + M_\Delta}{2M_\Delta} \left( \delta_{\sigma\tau} - \frac{\gamma_\sigma \gamma_\tau}{3} + \frac{2p_\sigma p_\tau}{3M_\Delta^2} - i \frac{p_\sigma \gamma_\tau - p_\tau \gamma_\sigma}{3M_\Delta} \right), \quad (36)$$

where all the  $\gamma$  matrices are in Euclidean space:  $\gamma_0 = \gamma_4$  and  $\gamma_k^M = -i\gamma_k^E$ .

Forming an appropriate ratio of the 3-point to the 2-point correlator serves to cancel out the unknown  $Z$ -factors and leading time-dependence. A particular product of 2-point correlators which minimizes the denominator noise-level is utilized as it contains smaller time-extents. The proposed ratios are:

$$R_{\sigma\mu\tau}^A(\Gamma^\nu, \vec{Q}, t) = \frac{G_{\sigma\mu\tau}^A(\Gamma, \vec{Q}, t)}{G_{kk}(\Gamma^4, \vec{0}, t_f)} \sqrt{\frac{G_{kk}(\Gamma^4, \vec{p}_i, t_f - t) G_{kk}(\Gamma^4, \vec{0}, t) G_{kk}(\Gamma^4, \vec{0}, t_f)}{G_{kk}(\Gamma^4, \vec{0}, t_f - t) G_{kk}(\Gamma^4, \vec{p}_i, t) G_{kk}(\Gamma^4, \vec{p}_i, t_f)}} \quad (37)$$

and

$$R_{\sigma\tau}^{PS}(\Gamma^\nu, \vec{Q}, t) = \frac{G_{\sigma\tau}^{PS}(\Gamma, \vec{Q}, t)}{G_{kk}(\Gamma^4, \vec{0}, t_f)} \sqrt{\frac{G_{kk}(\Gamma^4, \vec{p}_i, t_f - t) G_{kk}(\Gamma^4, \vec{0}, t) G_{kk}(\Gamma^4, \vec{0}, t_f)}{G_{kk}(\Gamma^4, \vec{0}, t_f - t) G_{kk}(\Gamma^4, \vec{p}_i, t) G_{kk}(\Gamma^4, \vec{p}_i, t_f)}}, \quad (38)$$

for the axial and pseudoscalar vertices. Summation over  $k = 1, 2, 3$  is implicit in the 2-point correlators. At large Euclidean time separations  $t_f - t$  and  $t$  these ratios become time-independent (plateau region).

$$R_{\sigma(\mu)\tau}^X(\Gamma^\nu, \vec{Q}, t) \longrightarrow C \Pi_{\sigma(\mu)\tau}^X = C \text{tr} [\Gamma^\nu \Lambda_{\sigma\sigma'}(0) \mathcal{O}_{\sigma(\mu)\tau}^X \Lambda_{\tau'\tau}(p)], \quad (39)$$

where  $X$  stands for the axial ( $A_\mu$ ) or pseudoscalar ( $P$ ) current. It is easy to show that the 2-point correlators are dominated by

$$G_{kk}(\Gamma^4, \vec{p}, t) = |Z|^2 e^{-E_{\Delta(p)}t} \frac{E_{\Delta(p)} + M_\Delta}{E_{\Delta(p)}} \left( 1 + \frac{\vec{p}^2}{3M_\Delta^2} \right) \quad (40)$$

and therefore the constant  $C$  is determined as

$$C \equiv \sqrt{\frac{3}{2}} \left[ \frac{2E_{\Delta(p_i)}}{M_{\Delta}} + \frac{2E_{\Delta(p_i)}^2}{M_{\Delta}^2} + \frac{E_{\Delta(p_i)}^3}{M_{\Delta}^3} + \frac{E_{\Delta(p_i)}^4}{M_{\Delta}^4} \right]^{-\frac{1}{2}}. \quad (41)$$

There are at most 256 available combinations of the Dirac and Lorentz indices in Equation (39), each one expressed as a linear combination of the axial (pseudoscalar) form factors times kinematical tensor coefficients. Since we are interested in the momentum dependence of the matrix elements, evaluation of the 3-point correlators is required for a large set of transition momenta  $\vec{q}$  for both  $A_{\mu}$  and  $P$  operators. In order to perform this economically we utilize the *sequential inversion through the sink* technique [23] by fixing the sink timeslice  $t_f$  and performing a backward sequential inversion through the sink. The sequential vector is coupled with a forward quark propagator and the Fourier transformed insertion operator at all intermediate time-slices  $0 \leq t \leq t_f$  at a small computational cost, obtaining thus the full momentum dependence of the amplitude. A drawback in this approach is the fact that the quantum numbers of the source and sink interpolators –which correspond to the Lorentz indices  $\sigma, \tau$  and  $\Gamma^{\nu}$  are now *fixed per sequential inversion*. Within the space of 64 available 3-point correlators corresponding to choices of  $\sigma, \tau$  and  $\nu$  we perform an *optimization by forming appropriate linear combinations* such as the degree of rotational symmetry of the summed correlator is maximal and consequently all transition momentum vectors  $\vec{q}$  that correspond to a fixed virtuality  $q^2$  will contribute to the form factor measurement in a rotationally symmetric fashion. This optimization technique has proved extremely useful in obtaining high accuracy results in the Nucleon elastic, Nucleon-to- $\Delta$  electromagnetic [22], axial and pseudoscalar transitions [21] as well as the  $\Delta$  electromagnetic form factors [23]. We evaluate the Dirac traces in Eq. (39) using symbolic software such as `form` [28] and Mathematica.

We construct the following two optimal linear combinations, which we refer to as Type-I and Type-II.

$$\text{Type - I :} \quad \Pi_{\mu}^{IA}(q) \equiv \sum_{i=1}^3 \sum_{\sigma, \tau=1}^3 \delta_{\sigma\tau} \text{tr} \left[ \Gamma^i \Lambda_{\sigma\sigma'}(0) \mathcal{O}_{\sigma'\mu\tau'}^{E,A} \Lambda_{\tau'\tau}(p) \right] \quad (42)$$

$$\text{Type - II :} \quad \Pi_{\mu}^{IIA}(q) \equiv \sum_{\sigma, \tau=1}^3 T_{\sigma\tau} \text{tr} \left[ \Gamma^4 \Lambda_{\sigma\sigma'}(0) \mathcal{O}_{\sigma'\mu\tau'}^{E,A} \Lambda_{\tau'\tau}(p) \right] \quad (43)$$

with the matrix  $T$ :

$$T_{\sigma\tau} = \begin{bmatrix} 0 & 1 & -1 \\ -1 & 0 & 1 \\ 1 & -1 & 0 \end{bmatrix}. \quad (44)$$

Detailed expressions for the decomposition of the above combinations to the four axial form factors are provided in Appendix B. The above types are in addition utilized for the extraction of the two pseudoscalar couplings (Appendix B). A large number ( $O(10^3)$ ) correlators of axial ( $A_{\mu}, \mu = 1, 2, 3, 4$ ) and pseudoscalar ( $P$ ) insertion momenta  $\vec{q}$  are combined for momentum transfers ranging up to  $\sim 3 \text{ GeV}^2$  per ensemble. We stress that *only two* sequential inversions through sink –one for each Type above– are required in order to disentangle completely all six form factors from the relevant 3-point functions.

Correlators corresponding to a fixed momentum transfer  $q^2$  are analyzed simultaneously in an overconstrained system analysis for the extraction of the form factors. Typically  $O(20 - 50)$  plateau averages for the optimal ratios given in Eq. (39) will contribute to the determination of the form factor for each  $Q^2$  value. A global  $\chi^2$ -minimization amounts technically to the singular value decomposition of an  $N \times M$  over-complete linear system, with  $M$  unknowns (4 for the axial or 2 for the pseudoscalar) and  $N$  input data (the  $O(20-50)$  plateau averages). Further details on this kind of analysis can be found in Ref [29]. Jackknife estimates are utilized for all levels of variance extraction on observables.

## B. Ensembles and Parameters

In Table I we summarize the parameters and number of configurations for the ensembles used in this work. As can be seen, three sets are employed. These are the same as the ones we used previously for the study of the nucleon axial form factors as well as the nucleon-to- $\Delta$  axial transition form factors. Therefore, these ensembles provide a complete calculation of the nucleon/ $\Delta$  sector, allowing a direct extraction of low energy couplings from a combined fit.

The gauge configurations used in the analysis include a set of quenched configurations on a  $32^3 \times 64$ , at  $\beta = 6.0$ , corresponding to a lattice spacing  $a = 0.092 \text{ fm}$  with pion masses 560 MeV, 490 MeV and 411 MeV. The low statistical noise makes this ensemble appropriate for checking our lattice methodology and some of the phenomenological



V	stat.	$m_\pi$ (GeV)	$m_N$ (GeV)	$m_\Delta$ (GeV)	$\kappa$
Quenched Wilson fermions					
$\beta = 6.0, a^{-1} = 2.14(6)$ GeV					
$32^3 \times 64$	200	0.563(4)	1.267(11)	1.470(15)	0.1554
$32^3 \times 64$	200	0.490(4)	1.190(13)	1.425(16)	0.1558
$32^3 \times 64$	200	0.411(4)	1.109(13)	1.382(19)	0.1562
Mixed action, $a^{-1} = 1.58(3)$ GeV					
Asqtad ( $am_{u,d/s} = 0.02/0.05$ ), DWF ( $am_{u,d} = 0.0313$ )					
$20^3 \times 64$	264	0.498(3)	1.261(17)	1.589(35)	
Asqtad ( $am_{u,d/s} = 0.01/0.05$ ), DWF ( $am_{u,d} = 0.0138$ )					
$28^3 \times 64$	550	0.353(2)	1.191(19)	1.533(27)	
Domain Wall Fermions (DWF)					
$m_{u,d}/m_s = 0.004/0.03, a^{-1} = 2.34(3)$ GeV					
$32^3 \times 64$	1428	0.297(5)	1.27(9)	1.455(17)	

TABLE I: Ensembles and parameters used in this work. We give in the first column the lattice size, in the second the statistics, in the third, fourth and fifth the pion, nucleon and  $\Delta$  mass in GeV respectively. We did not do a full form-factor analysis on the  $20^3 \times 64$  mixed-action ensemble. Rather we merely determined the axial matrix element at  $q^2 = 0$  (a much cheaper computation) for our axial charge chiral fits.

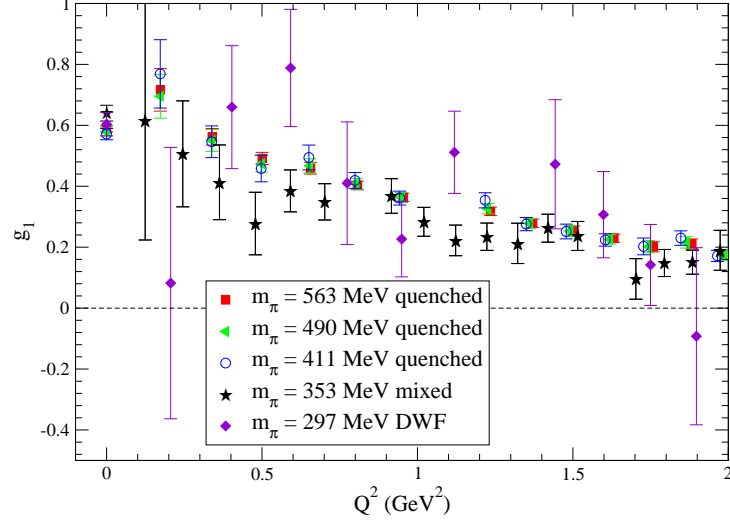
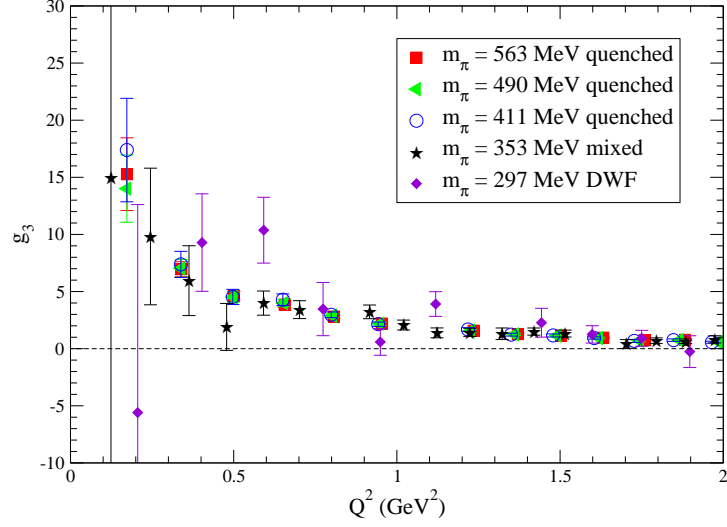
relations. We apply Gaussian smearing at the source and sink in order to minimize the excited state contamination on the baryon correlators. The parameters  $\alpha = 4.0$  and  $n = 50$  have been tuned to provide optimal overlap to a nucleon state [21]. The source-sink separation is set at  $\Delta T = 12a = 1.1$  fm. In our previous studies involving the  $\Delta$  such a time separation was found sufficient for ground state dominance. The second set consists of two ensembles that use two degenerate light and one strange ( $N_f = 2 + 1$ ) Asqtad-improved dynamical staggered fermions generated by the MILC collaboration [30]. The strange quark mass is fixed to its physical value, the lattice spacing is set to 0.124 fm and the lowest pion mass is 353 MeV. Our calculation employs Domain Wall (DW) valence quarks with light quark mass tuned so as the pion mass matches the lowest pion mass obtained using staggered fermions. The extent of the fifth dimension of the domain wall action is set to  $L_5 = 16a$ , which was demonstrated to provide minimal violations to the chiral symmetry properties of the domain wall fermion (DWF) operator. The source-sink separation is set to  $\Delta T = 8a = 1.0$  fm and Gaussian smearing is applied at the source and sink with APE smearing on gauge links that enter the smearing function applied on the interpolating fields. The parameters are given in Ref. [21]. Finally, the third set is an  $N_f = 2 + 1$  ensemble of DWF generated by the RBC-UKQCD collaborations [31] with a lattice spacing  $a = 0.084$  fm and the physical volume of  $(2.7 \text{ fm})^3$  and pion mass of 0.297 MeV. The extent of the fifth dimension is also here  $L_5 = 16a$ . It turns out that the residual quark mass introduced via the chiral symmetry breaking effects is  $am_{\text{res}} = 0.000665(3)$ , or 17% of the bare quark mass. The smearing parameters for the interpolating fields are given in Ref. [22]. The sink-source time separation is set at  $\Delta T = 12a = 1.01$  fm. In order to increase the statistics at this lowest pion mass we use the *coherent sink technique*, employed in our study of the nucleon to  $\Delta$  transition using the same ensemble [22]. The four quark sources are placed at timeslice  $t_i = (i - 1)16, i = 1, \dots, 4$  for each configuration. Four forward propagators must be computed – each with a source at one of the time-slices. The  $\Delta$  sinks are constructed at all four equally spaced time-slices  $t_f(i) = t_i + 12$  and one sequential inversion is performed in order to construct the three-point correlator. Gauge invariance ensures that combining the sequential vector with each one of the forward quark propagators generated at  $t_i$ , projects the appropriate  $\Delta$  matrix element between  $t_i$  and  $t_i + 12$  as the other cross-terms will average to zero. It has been shown in Ref. [22] that while statistics is thus multiplied by 4, the noise level is not raised above what expected from the four completely independent correlators which participate in the coherent sink. This means that we can reduce the error by a factor of two at the cost of one sequential inversion. Therefore the 1428 statistics given in the table correspond to 357 coherent sequential inversions per each type of combinations (see Eq. (43)).

## IV. RESULTS

### A. Axial-vector and Pseudoscalar Form Factors

In this section we present results on the  $\Delta$  axial-vector and pseudoscalar form factors from the ensembles utilized in this work. The axial current is renormalized multiplicatively in all ensembles. Values for the renormalization constant

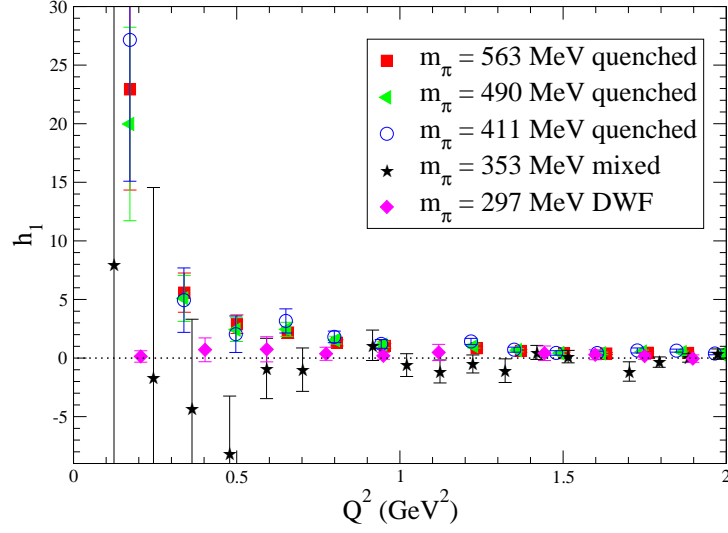
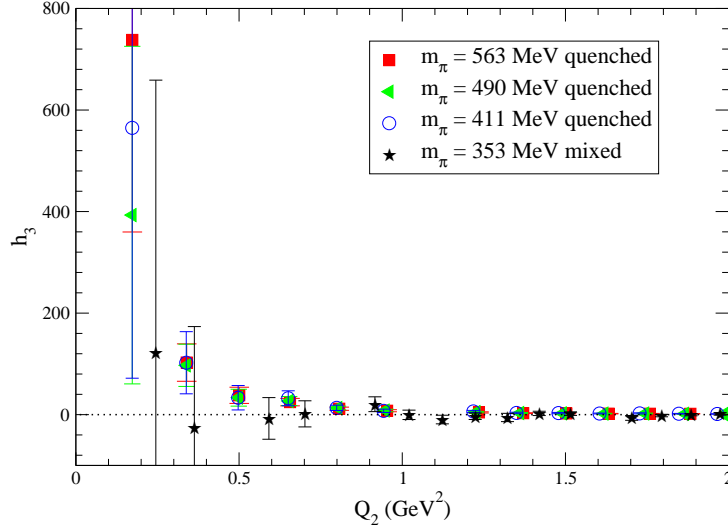


FIG. 1: Lattice QCD results for the  $g_1$  axial form-factor.FIG. 2: Lattice QCD results for the  $g_3$  axial form-factor.

$Z_A$  are provided in Table II.

In Figs. 1, 2, 3 and 4 we show the results for the four axial form factors,  $g_1$ ,  $g_3$ ,  $h_1$  and  $h_3$ , respectively. All the results on these form factors are provided in Appendix C. The form factor  $g_1$  is the dominant axial-vector form factor and the only one that can be extracted directly from the matrix element at  $Q^2 = 0$ , determining the axial charge of the  $\Delta$ . Based on PCAC and pion pole dominance we expect  $g_1$  to be a smooth function of  $Q^2$ , whereas  $h_1$  and  $g_3$  to have a pion-pole and  $h_3$  a double pion-pole behavior. Given that  $g_1$  and  $h_1$  are multiplied by  $Q^2$ , whereas  $h_3$  is multiplied by  $Q^4$  it is increasingly more difficult to resolve these form factors via the simultaneous overconstrained analysis of the measured matrix element of the axial-vector current, especially at small  $Q^2$  – a fact that is clearly reflected on the statistical error of the form factors shown in the figures. The results from the quenched ensemble, although based on the analysis of 200 configurations, have the lowest statistical noise and this is the primary reason for using them in this first calculation of the form factors. The statistical noise is more severe for the DWF ensemble at  $m_\pi = 297$  MeV for which results on  $h_3$  are too noisy to be useful and are omitted from plots. We do, however, include these numbers in the tables in the Appendix C for completeness.

Figs. 5 and 6 show the pseudoscalar form factors  $\tilde{g}$  and  $\tilde{h}$ , respectively, as defined in Eq. (10), where the pion pole is explicitly written. The numerical values of these form factors are provided in Appendix C. As confirmed

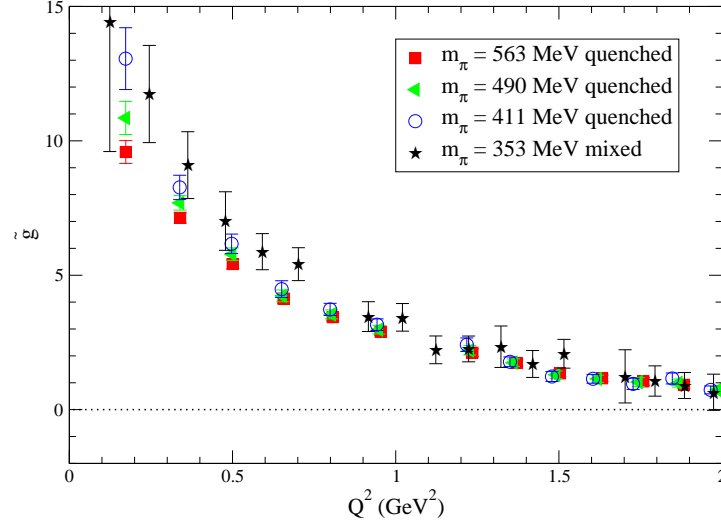
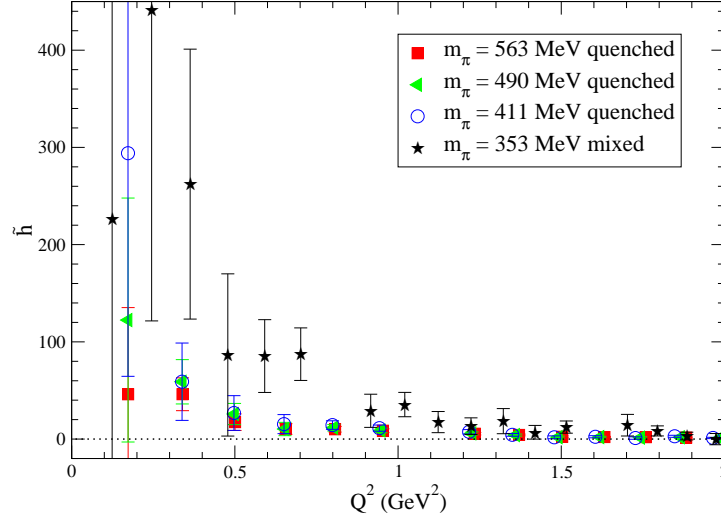
FIG. 3: Lattice QCD results for the  $h_1$  axial form-factor.FIG. 4: Lattice QCD results for the  $h_3$  axial form-factor.

by the numerical results,  $\tilde{g}$  is the dominant pseudoscalar form factor showing a pion-pole dependence, whereas the subdominant form factor  $\tilde{h}$  shows a stronger  $Q^2$ -dependence consistent with a double pion-pole. In section II we already defined the physically relevant pion- $\Delta$  coupling  $G_{\pi\Delta\Delta}(m_\pi^2)$  factoring out the pion-pole and fixing coefficients via PCAC through Eq. 14.  $G_{\pi\Delta\Delta}(q^2)$  has a finite value at the origin, as can be seen in Fig. 7 where numerical results are depicted. This value in fact defines the traditional strong coupling  $g_{\pi\Delta\Delta}$  of the pion to the  $\Delta$  state via

$$g_{\pi\Delta\Delta} = G_{\pi\Delta\Delta}(m_\pi^2). \quad (45)$$

The secondary momentum-dependent coupling,  $H_{\pi\Delta\Delta}(Q^2)$ , is plotted in Fig. 8. The numerical results are consisted with a pion-pole divergence at small  $Q^2$  as expected from the analysis given in the previous section. The statistical error on this coupling is larger in particular at small  $Q^2$  since in the combined analysis the pseudoscalar matrix element is multiplied by a factor of  $Q^2$ .

Notice that the extraction of  $G_{\pi\Delta\Delta}$  and  $H_{\pi\Delta\Delta}$  from Eqs. (14) and (15) requires knowledge of the light quark mass  $m_q$  and the pion decay constant,  $f_\pi$ , on each of the ensembles. Calculation of  $f_\pi$  requires the two-point functions of

FIG. 5: Lattice QCD results for the  $\tilde{g}$  pseudoscalar form-factor.FIG. 6: Lattice QCD results for the  $\tilde{h}$  pseudoscalar form-factor.

the axial-vector current  $A_4^3$  with local-smeared (LS) and smeared-smeared (SS) quark sources,

$$C_{LS}^A(t) = \sum_{\mathbf{x}} \langle \Omega | T \left( A_4^3(\mathbf{x}, t) \tilde{A}_4^3(\mathbf{0}, 0) \right) | \Omega \rangle \quad (46)$$

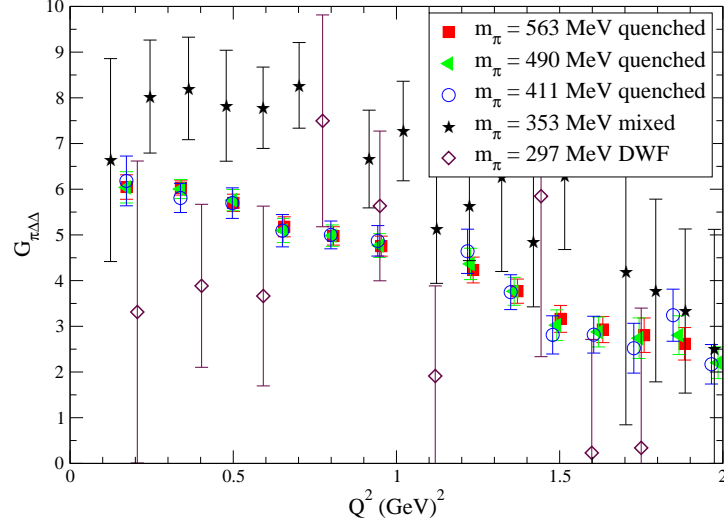
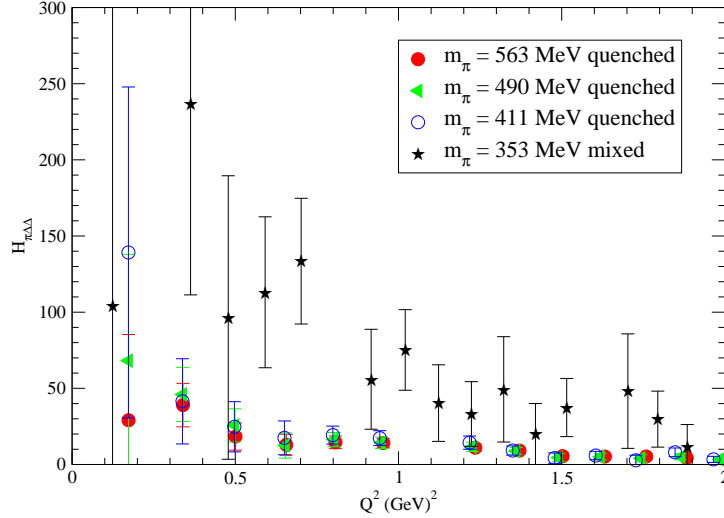
(and similarly for  $C_{SS}^A$ ), where  $A_4^3(\mathbf{x}, t)$  denotes the local operator and  $\tilde{A}_4^3(\mathbf{x}, t)$  the smeared operator. The pion decay constant  $f_\pi$  is obtained from the pion-to-vacuum matrix element

$$\langle 0 | A_\mu^a(0) | \pi^b(p) \rangle = i f_\pi p_\mu \delta^{ab} \quad (47)$$

extracted from the ratio of the two-point functions  $C_{LS}^A$  and  $C_{SS}^A$  and

$$f_\pi^{\text{eff}}(t) = Z_A \sqrt{\frac{2}{m_\pi}} \frac{C_{LS}^A(t)}{\sqrt{C_{SS}^A(t)}} e^{m_\pi t/2}. \quad (48)$$

in the large Euclidean time limit.

FIG. 7: Lattice QCD results for the primary  $\pi\Delta\Delta$  coupling,  $G_{\pi\Delta\Delta}$ .FIG. 8: Lattice QCD results for the secondary  $\pi\Delta\Delta$  coupling,  $H_{\pi\Delta\Delta}$ .

The renormalized quark mass  $m_q$  is determined from AWI, via two-point functions of the pseudoscalar density with either local ( $P^3$ ) or smeared ( $\tilde{P}^3$ ) quark fields,

$$C_{LS}^P(t) = \sum_{\mathbf{x}} \langle \Omega | T \left( P^3(\mathbf{x}, t) \tilde{P}^3(\mathbf{0}, 0) \right) | \Omega \rangle, \quad (49)$$

(and similarly for  $C_{SS}^P$ ). The effective quark mass is defined by

$$m_{\text{eff}}^{\text{AWI}}(t) = \frac{m_\pi}{2} \frac{Z_A}{Z_P} \frac{C_{LS}^A(t)}{C_{LS}^P(t)} \sqrt{\frac{C_{SS}^P(t)}{C_{SS}^A(t)}}. \quad (50)$$

and its plateau value yields  $m_q$ . Note that  $Z_P$  will be needed only if ones wants  $m_q$  alone. Since  $Z_P$  enters also Eq. (13), it cancels –as does  $Z_A$  since it comes with  $f_\pi$ – and therefore  $G_{\pi\Delta\Delta}$  and  $H_{\pi\Delta\Delta}$  are extracted directly from ratios of lattice three- and two-point functions without prior knowledge of either  $Z_A$  or  $Z_P$ . We also note that the quark mass computed through (50) includes the effects of residual chiral symmetry breaking from the finite extent  $L_5$  of the fifth dimension. These effects are of the order of 17% for the DWF ensemble and 15% for the hybrid ensemble

$\kappa$ or $am_l$	$am_q$	$af_\pi/Z_A$	$Z_A$
Quenched Wilson fermions			
0.1554	0.0403(4)	0.0611(14)	0.808(7)
0.1558	0.0307(4)	0.0587(16)	0.808(7)
0.1562	0.0213(4)	0.0563(17)	0.808(7)
Hybrid or mixed action			
0.02	0.0324(4)	0.0648(8)	1.0994(4)
0.01	0.0159(2)	0.0636(6)	1.0847(6)
$N_F = 2 + 1$ DWF			
0.004	0.004665(3)	0.06575(12)	0.74521(2)

TABLE II: The first column gives the hopping parameter  $\kappa$  for Wilson fermions or the lattice mass of the domain wall fermion, the second the renormalized quark mass, the third the unrenormalized pion decay constant  $f_\pi/Z_A$  in lattice units, and the fourth the axial current renormalization constant  $Z_A$ .

(also referred to as mixed scheme). Chiral symmetry breaking affects the PCAC relations and therefore the value of both strong couplings  $G_{\pi\Delta\Delta}$  and  $H_{\pi\Delta\Delta}$  through Eq. (13).

### B. Testing Pion-Pole Dominance in the Axial and Pseudoscalar Matrix Element

In this section we examine in detail the pion-pole dependence expected for the  $\Delta$  form factors by performing fits to the results obtained. First, we test the validity of the Goldberger-Treiman relations of Eqs. (23, 24) by evaluating the ratios

$$\frac{f_\pi G_{\pi\Delta\Delta}(q^2)}{M_\Delta g_1(q^2)} \quad (51)$$

and

$$\frac{f_\pi H_{\pi\Delta\Delta}(q^2)}{M_\Delta h_1(q^2)}. \quad (52)$$

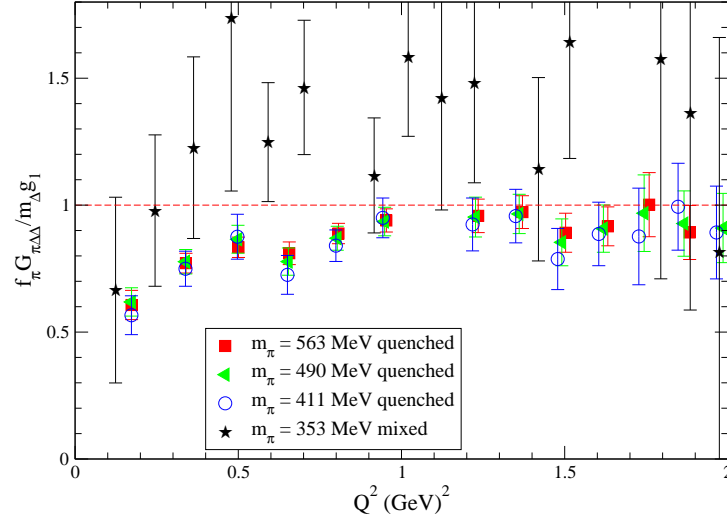
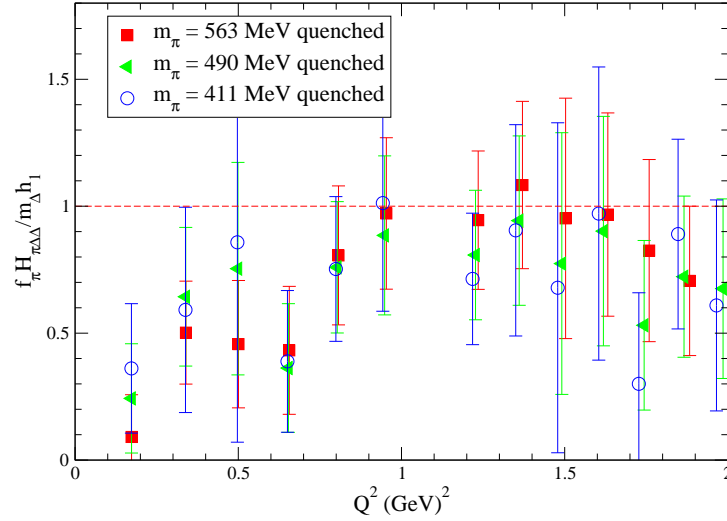
These relations are expected to hold at low  $Q^2$ . We show the results in Figs. 9 and 10. The first ratio, given in Eq. (51), carries moderate statistical error. It is consistent with unity for  $Q^2 \gtrsim 0.8 \text{ GeV}^2$  for the quenched ensembles while it is underestimated at smaller  $Q^2$  values. This discrepancy at smaller  $Q^2$  can be attributed to chiral effects on  $G_{\pi\Delta\Delta}$ , which is expected to be more seriously affected by pion cloud effects than  $g_1$ . The results using the hybrid dynamical ensemble, on the other hand, are consistently higher than unity for  $Q^2 > 0.5 \text{ GeV}^2$ . The large statistical errors carried by these data make it difficult to draw definite conclusions. The behavior of this ratio is very similar to the behavior shown by the corresponding ratio for the nucleon GT relation as well as the nucleon-to- $\Delta$  axial transition [21].

The second GT-type relation, given in Eq. (52), is statistically consistent with unity for the quenched results and  $Q^2 > 0.8 \text{ GeV}^2$ . The results from the dynamical ensembles are plagued by too large statistical noise to be able to meaningfully display them on the plot. We therefore have omitted these data from Fig. 10. A very similar and consistent behavior with the first ratio is observed for the quenched data. We remind the reader that it is the first Goldberger-Treiman relation that is more significant for phenomenology, as it is this relation that connects the axial charge (from  $g_1$  at  $Q^2 = 0$ ) to the  $G_{\pi\Delta\Delta}$  coupling.

To further probe the pion pole assumptions entering into our derivation of the GT relations we perform a set of fits to our form factor data. We have no *a priori* theoretical expectation for the functional form of  $g_1(q^2)$ , although typically a dipole form seems to accommodate well the nucleon axial form factor  $G_A$  as well as the leading axial  $N - \Delta$  transition form factor  $C_5^A$ . We note however that there seems to be a small dip in the  $g_1$  at  $q^2 = 0$  for the quenched ensembles. To accommodate this we fit the data to:

$$g_1(Q^2) = \frac{a + bQ^2}{(Q^2 + m_1^2)^3} \quad (53)$$

The resulting fits are shown in Fig. 11. The values for the fitted parameters are given in Table III. We note that the mass parameter  $m_1$  determining the slope as  $Q^2 \rightarrow 0$  is around 1 GeV, a scale typical for axial dipole masses controlling the dependence of nucleon  $G_A$  and the dominant axial  $N - \Delta$   $C_5^A$  form factor.

FIG. 9: Ratio test of the Goldberger-Treiman Relation for  $G_{\pi\Delta\Delta}$ .FIG. 10: Ratio test of the Goldberger-Treiman Relation for  $H_{\pi\Delta\Delta}$ .

We consider the form

$$\left[ \frac{a + bQ^2}{(Q^2 + m_1^2)^3} \right] \frac{c}{(Q^2 + m_2^2)} \quad (54)$$

for  $g_3$  based on the pion pole dominance prediction given in Eq.(25). The parameters  $a$ ,  $b$ , and  $m_1$  are fixed to the values arising from the fit of the  $g_1$  data using the Ansatz given in Eq. (53). The fits are shown in Fig. 12. The fitted parameters are given in Table IV. Note that the value of  $m_2$  is considerably smaller compared to  $m_1$ , as in fact is expected since this is detected from the presence of the pion-pole. This is especially verified by the quenched data where  $m_2$  is close to the actual pion mass  $m_{\pi}$  of the ensemble.

Pion pole dominance fixes completely the ratio  $g_3/g_1$

$$\frac{g_3}{g_1} = \frac{4M_{\Delta}^2}{m_{\pi}^2 - q^2}. \quad (55)$$

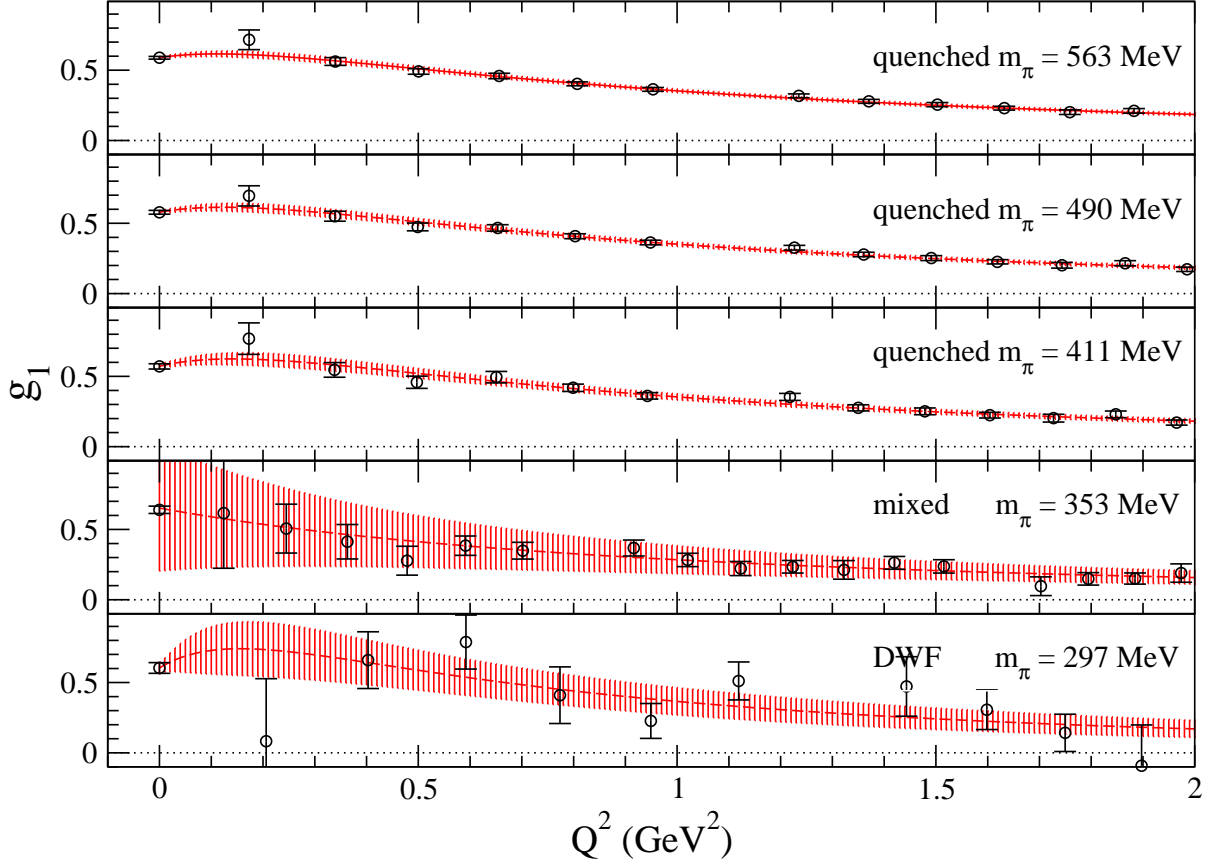


FIG. 11: Fits to the data for the  $g_1$  form-factor using the form given in Eq. 53.

We form the ratio  $g_3/g_1$  from our data and fit separately to a monopole form:

$$\frac{c}{(Q^2 + m_2^2)} . \quad (56)$$

This fit is displayed in Fig. 13. Using a ratio eliminates any need to know the theoretical form for  $g_1(q^2)$  alone. The fitted parameters  $c$  and  $m_2$  are given in Table V. The verification of the predicted form given in Eq. (55) is very good, with the pole mass  $m_2$  consistent with the pion mass and the constant  $c$  reasonably close to  $4M_\Delta^2$ .

The form factor  $h_1$  is similar to  $g_3$  having a pion-pole dependence. We display the ratio  $h_1/g_3$  in Fig. 14 for the quenched QCD ensembles. This ratio is notably constant over the whole  $Q^2$  range above  $0.4 \text{ GeV}^2$ , with the constant  $\sim 0.5$ . Based on this observation, we use the Ansatz given in Eq. (54) also for  $h_1$ . The fit is shown in Fig. 15 and the fitted parameters are given in Table VI. Again,  $m_2$  is considerably smaller compared to  $m_1$ , in accordance to the presence of a light (pion) mode.

From Eq. (26), the ratio  $h_3/h_1$  is completely fixed:

$$\frac{h_3}{h_1} = \frac{4M_\Delta^2}{m_\pi^2 - q^2} . \quad (57)$$

We plot this ratio in Fig. 16. Fitting the data to the monopole form of Eq. (56), we get parameters  $m_2$  and  $c$  within the range of the expected value (Eq. 57) – see Table VII indicating that the subdominant form factor diverges with a double pion-pole-dependence.

In Fig. 17 we present the fit of  $h_3$  to the Ansatz

$$\left[ \frac{a + bQ^2}{(Q^2 + m_1^2)^3} \right] \frac{d}{(Q^2 + m_2^2)^2}, \quad (58)$$



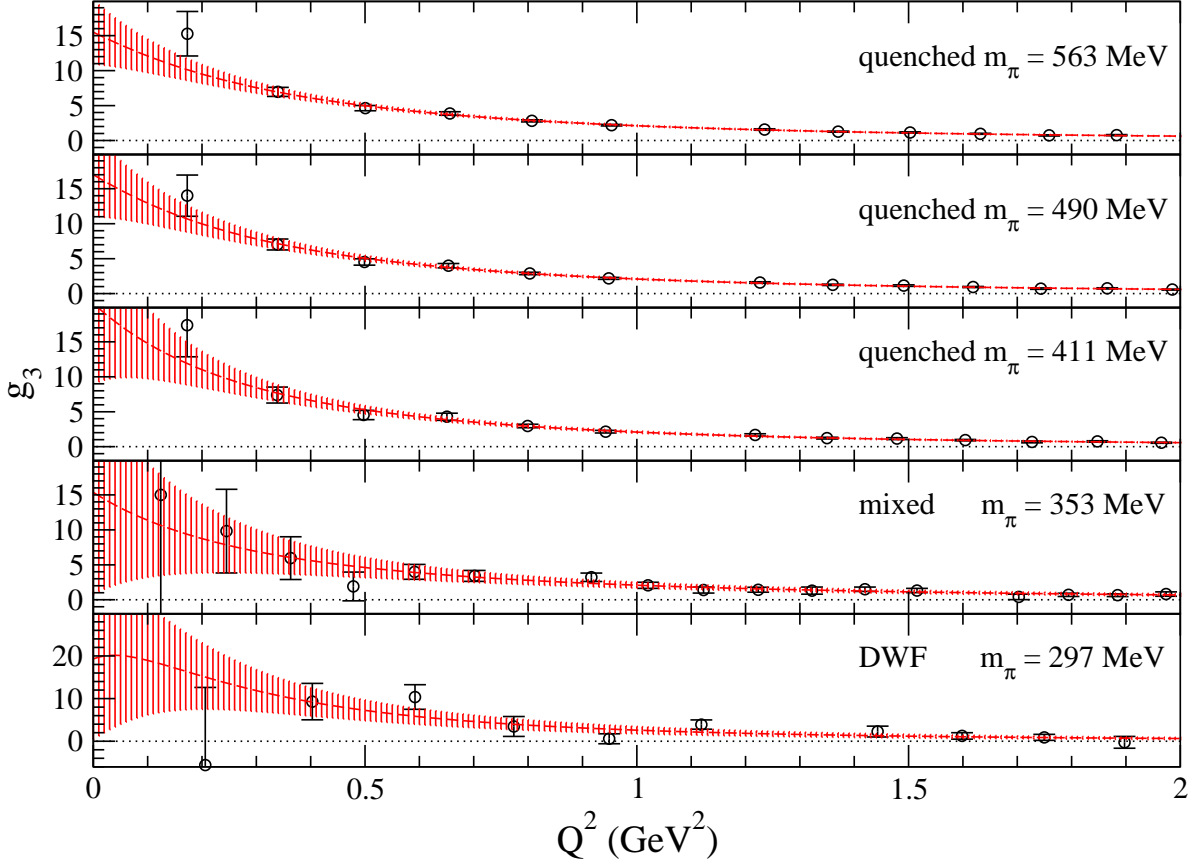


FIG. 12: Fits to the data for the  $g_3$  form-factor using the form given in Eq. 54.

with  $a$ ,  $b$ , and  $m_1$  fixed to the values extracted from the fit of  $g_1$ . The fitted parameters  $d$  and  $m_2$  are given in Table VIII, in accordance to the  $h_3/h_1$  fit (Table VII).

In the pseudoscalar sector, one expects a monopole dependence also for the ratio  $\tilde{h}/\tilde{g}$ . Fitting the data to the monopole form of Eq. (56), we get the parameters provided in Table IX. Indeed, an agreement of the  $m_2$  pole mass to the pion mass within the allowed by statistical noise regime is seen.

The overall conclusion from the fits in this section is that all form factors satisfy qualitatively the pion-pole dependence predicted by PCAC. This is most clearly exemplified in the case of quenched QCD where the level of statistical noise allows such detailed analysis. In all cases the data fit these forms to good confidence levels, i.e.,  $\chi^2/\text{dof} \lesssim 1$ . Enhanced statistical noise for the dynamical ensembles limits the verification to the dominant form factors only, as the subdominant ones are beyond reach, but this still is a useful result as it shows the consistency between quenched and dynamical results. This corroborates other baryon studies that show small effects due to dynamical quark for pion masses larger than about 300 MeV.

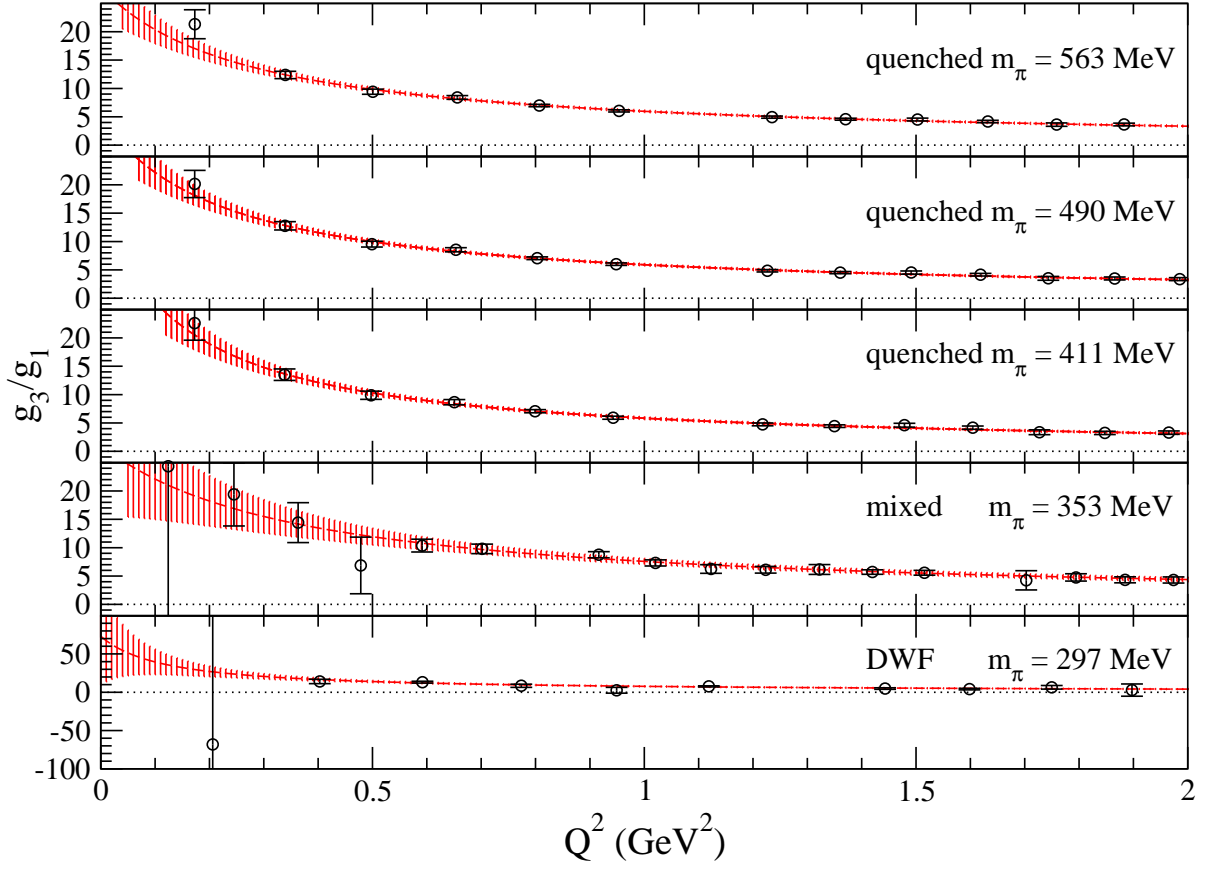


FIG. 13: Monopole fits as given by Eq. 56 to the ratio  $g_3/g_1$ .

$m_\pi$ (GeV)	$a$	$b$	$m_1$ (GeV)	$\chi^2/\text{dof}$
quenched Wilson fermions				
0.563	0.53(18)	2.15(31)	0.98(5)	0.82
0.490	0.47(18)	2.08(33)	0.99(6)	1.07
0.411	0.40(19)	1.98(38)	0.94(8)	1.48
mixed action				
0.353	3.0(22.0)	2.4(1.9)	1.3(1.2)	0.44
domain wall fermions				
0.297	0.19(24)	1.5(9)	0.82(18)	1.1

TABLE III: Fit parameters for  $g_1(Q^2)$  using Eq. 53.

$m_\pi$ (GeV)	$c$	$m_2$ (GeV)	$\chi^2/\text{dof}$
quenched Wilson fermions			
0.563	7.77(88)	0.54(11)	0.61
0.490	7.45(89)	0.50(11)	0.55
0.411	7.1(1.0)	0.44(15)	0.65
mixed action			
0.353	10.7(4.6)	0.67(43)	0.49
domain wall fermions			
0.297	10.0(5.3)	0.56(37)	1.26

TABLE IV: Fit parameters for  $g_3(Q^2)$  using Eq. 54. Parameters  $a$ ,  $b$  and  $m_1$  are fixed with the results of  $g_1$  fits in Table III.

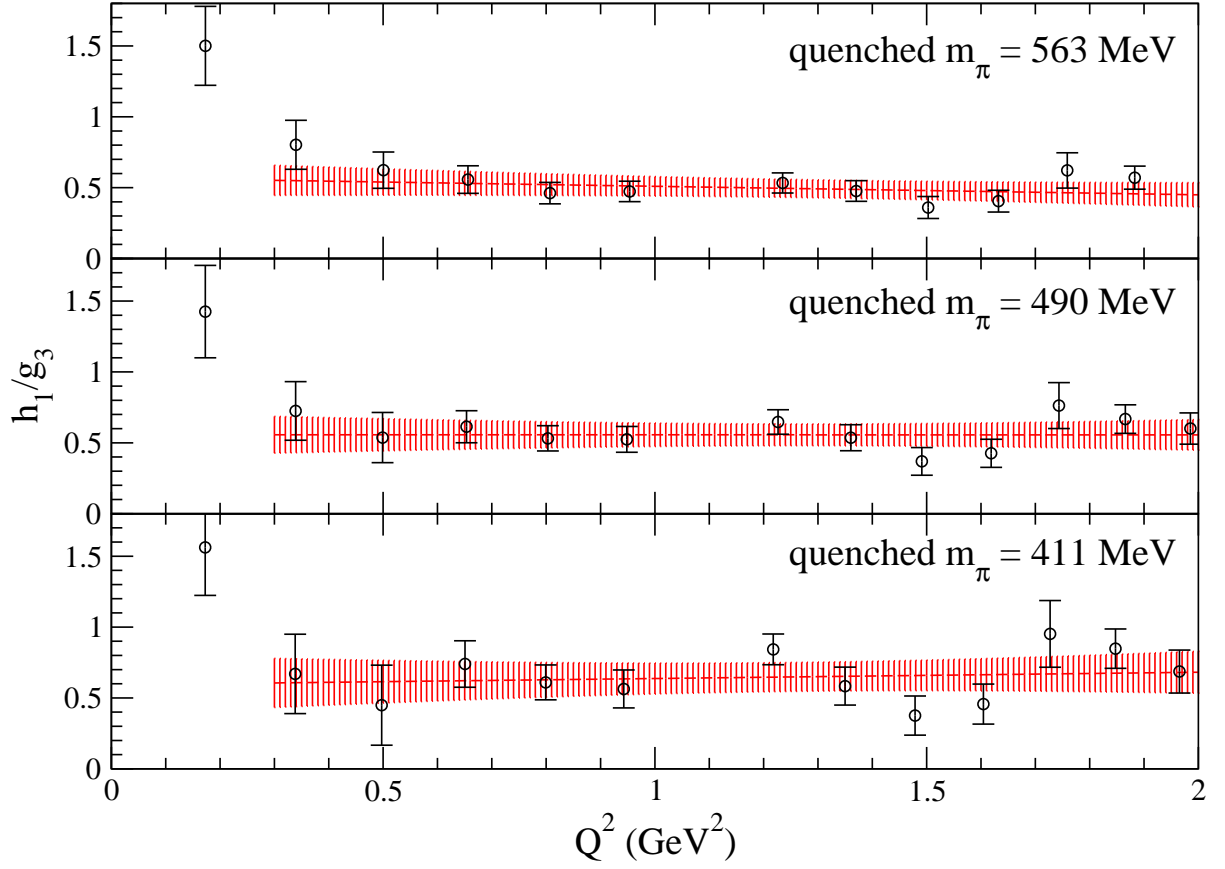


FIG. 14: The ratio  $h_1/g_3$  as a function of  $Q^2$ , with unity marked with a red line.

$m_\pi$ (GeV)	$m_2$ (GeV)	$c$	$4M_\Delta^2$ (GeV <sup>2</sup> )	$\chi^2/\text{dof}$
quenched Wilson fermions				
0.563	0.523(64)	7.60(52)	8.64(18)	0.67
0.490	0.477(63)	7.25(49)	8.12(18)	0.54
0.411	0.396(75)	6.76(48)	7.64(21)	0.60
mixed action				
0.353	0.61(18)	10.4(1.6)	9.40(33)	0.34
domain wall fermions				
0.297	0.34(17)	8.6(1.3)	5.82(20)	0.66

TABLE V: Fit parameters for  $g_3(Q^2)/g_1(Q^2)$  using the monopole form of Eq. 56.

$m_\pi$ (GeV)	$c$	$m_2$ (GeV)	$\chi^2/\text{dof}$
quenched Wilson fermions			
0.563	3.04(48)	$2 \times 10^{-8} (8 \times 10^{-7})$	1.32
0.490	3.32(84)	0.03(81)	1.37
0.411	3.8(1.8)	0.1(1.4)	1.52

TABLE VI: Fit parameters for  $h_1(Q^2)$  using Eq. 54. Parameters  $a$ ,  $b$  and  $m_1$  are fixed with the results of  $g_1$  fits in Table III.

$m_\pi$ (GeV)	$m_2$ (GeV)	$c$	$4M_\Delta^2$ (GeV <sup>4</sup> )	$\chi^2/\text{dof}$
quenched Wilson fermions				
0.563	0.26(17)	7.6(1.1)	8.64(18)	0.21
0.490	0.31(19)	7.4(1.1)	8.12(18)	0.38
0.411	0.28(25)	6.7(1.1)	7.64(21)	0.58

TABLE VII: Fit parameters for  $h_3(Q^2)/h_1(Q^2)$  using the monopole form of Eq. 56.

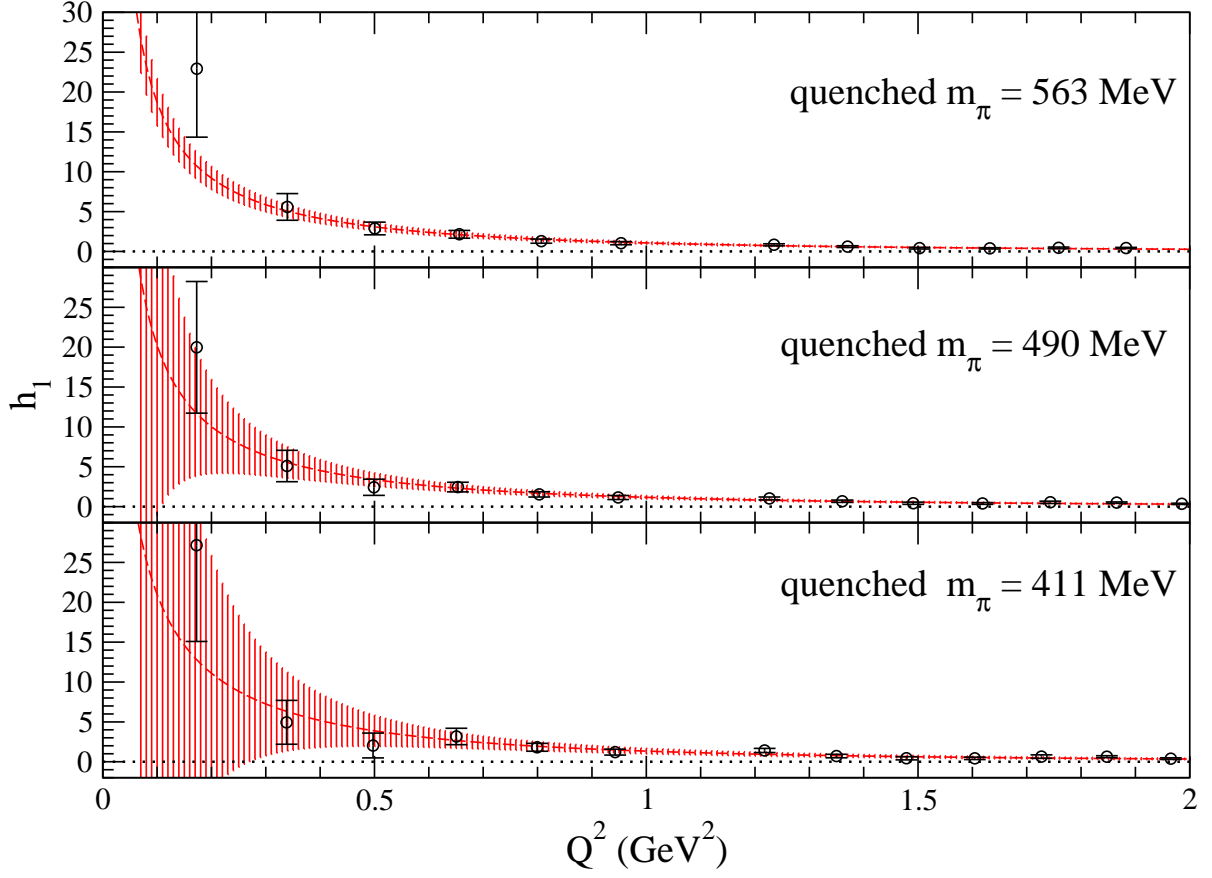


FIG. 15: Fits to the data for the  $h_1$  form-factor using the form given in Eq. 54.

$m_\pi$ (GeV)	$d$	$m_2$ (GeV)	$\chi^2/\text{dof}$
quenched Wilson fermions			
0.563	22(6)	0.03(58)	0.46
0.490	26(10)	0.25(28)	0.35
0.411	28(15)	0.28(43)	0.33

TABLE VIII: Fit parameters for  $h_3(Q^2)$  using Eq. 58. Parameters  $a$ ,  $b$  and  $m_1$  are fixed with the results of  $g_1$  fits in Table III. The dynamical fermion data sets contain too much noise for the fits to be useful.

$m_\pi$ (GeV)	$m_2$ (GeV)	$c$	$\chi^2/\text{dof}$
quenched Wilson fermions			
0.563	0.73(39)	4.2(1.6)	0.23
0.490	0.42(43)	3.3(1.2)	0.22
0.411	0.45(70)	3.9(2.0)	0.32

TABLE IX: Fit parameters for  $\tilde{h}(Q^2)/\tilde{g}(Q^2)$  using the monopole form of Eq. 56.

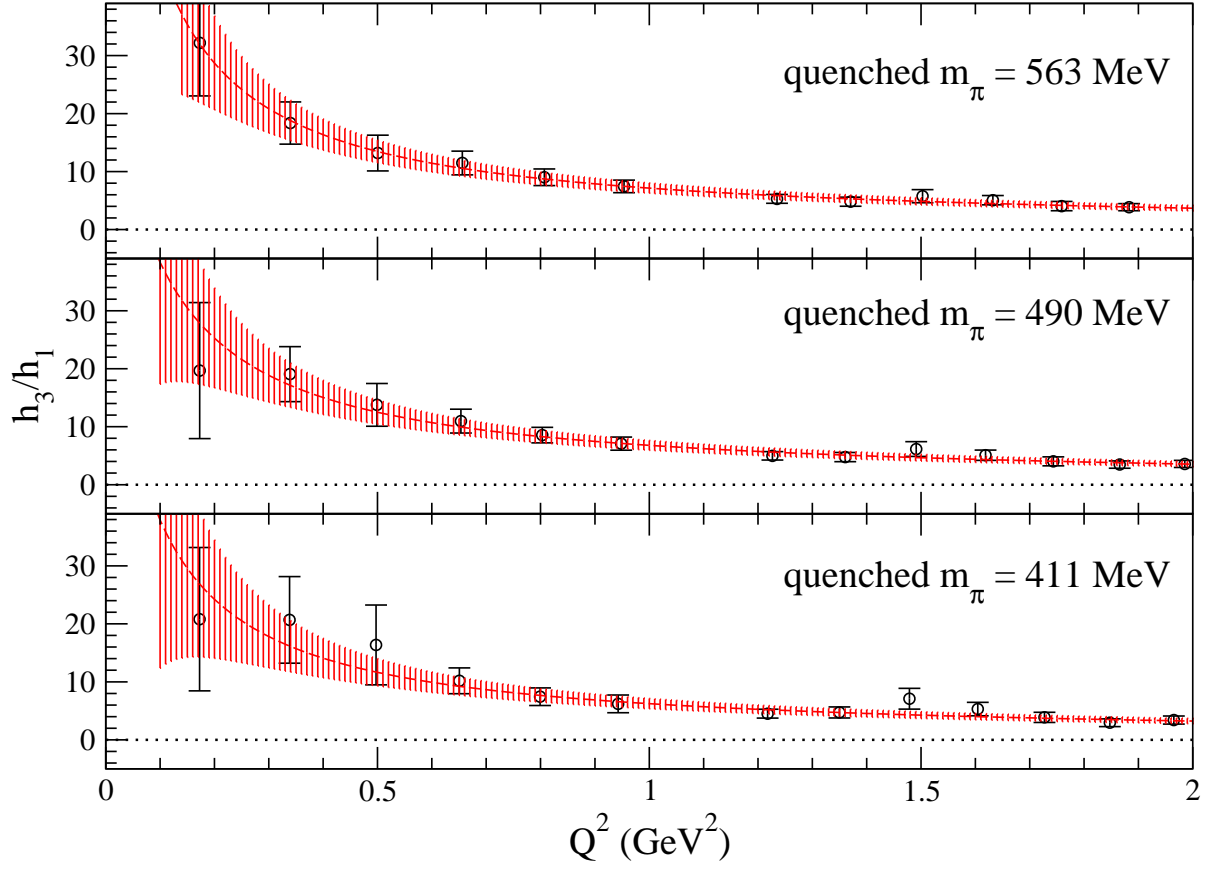


FIG. 16: Monopole fits to the ratio  $h_3/h_1$  as described by Eq. 56.

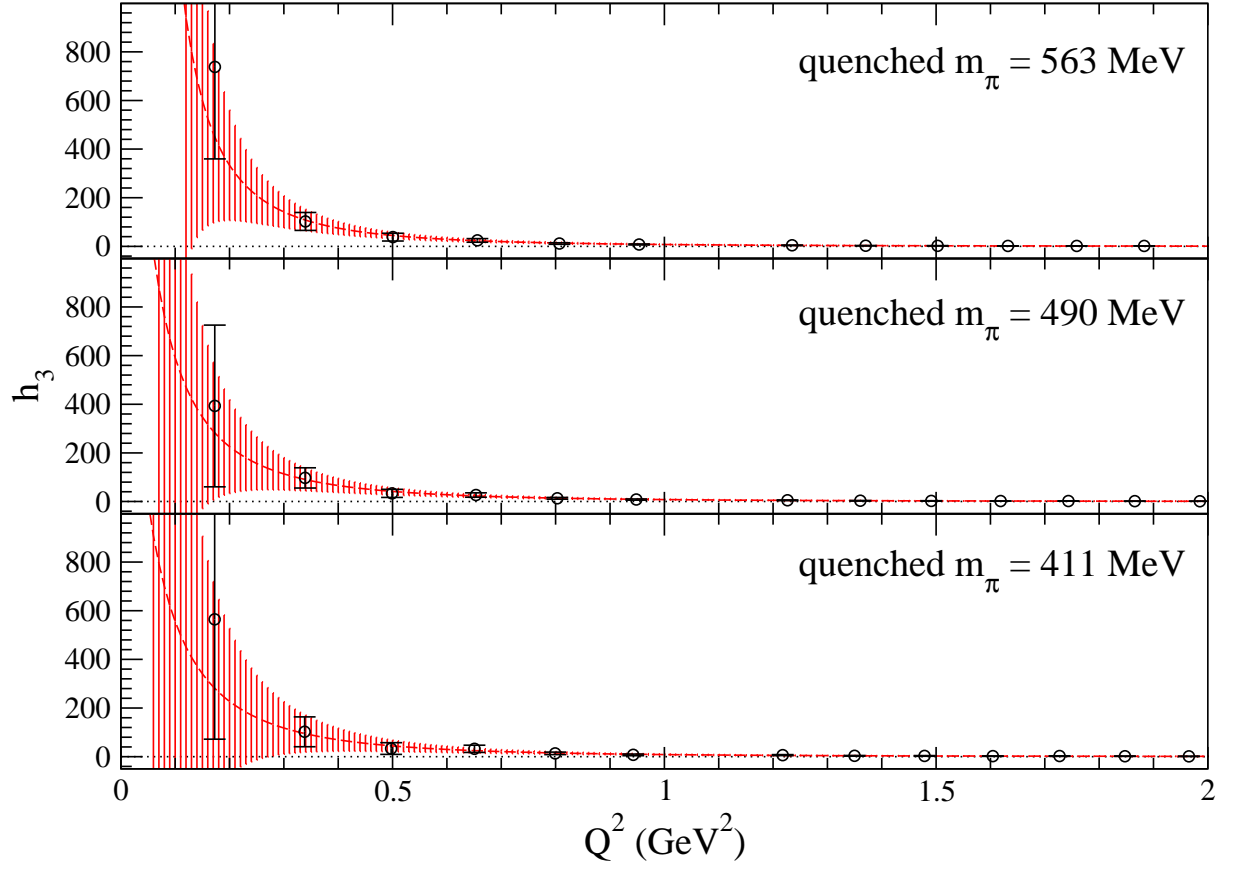


FIG. 17: Fits to the data for the  $h_3$  form-factor using the form given in Eq. 58.

$m_\pi$ (GeV)	$g_1(0)$
Quenched	
0.563(4)	0.589(10)
0.490(4)	0.578(13)
0.411(4)	0.571(18)
Mixed action	
0.498(3)	0.573(23)
0.353(2)	0.640(26)
DWF	
0.297(5)	0.604(38)

TABLE X: Numerical values for the dominant form factor  $g_1(0)$  on each of the ensembles.  $G_{\Delta\Delta} = -3g_1(0)$  with our normalization.

## V. PHENOMENOLOGICAL COUPLINGS OF THE $\Delta$ AND COMBINED CHIRAL FIT

Crucial parameters in heavy baryon chiral effective theories (HB $\chi$ PT) with explicit  $\Delta$  degrees of freedom are the axial couplings of the nucleon,  $g_A$ , the axial  $N - \Delta$  transition coupling,  $c_A$ , and the axial charge of the  $\Delta$ ,  $g_{\Delta\Delta}$ . Assuming PCAC, these can be related via GT relations to the effective  $\pi NN$ ,  $\pi N\Delta$  and  $\pi\Delta\Delta$  strong couplings:

$$g_A = \frac{f_\pi}{M_N} g_{\pi NN} \quad , \quad c_A = \frac{f_\pi}{M_N} g_{\pi N\Delta} \quad , \quad g_{\Delta\Delta} = \frac{f_\pi}{M_\Delta} g_{\pi\Delta\Delta} \quad (59)$$

We note that alternative notation and normalization factors exist in the literature in the definition of the effective strong couplings for  $\pi N\Delta$  and  $\pi\Delta\Delta$ . In addition, note that in such schemes Eqs. (59) are actually *defining* relations for the strong couplings.  $g_A$  is very well known experimentally and a variety of lattice and theoretical calculations offer precise estimates.  $c_A$  is much less-well determined, via the parity violating N-to- $\Delta$  amplitude which connects it to the dominant axial transition form factor  $C_5^A(q^2)$ .  $g_{\Delta\Delta}$  remains undetermined from experiment and is typically treated –as is also the case for  $c_A$ – as a fit parameter to be determined from fits to experimental or lattice data.

There have been several sum-rules calculations of the effective  $\pi\Delta\Delta$  coupling [32–34]. In Ref. [35] symmetry arguments in a quartet scheme where  $N_+^*$ ,  $N_-^*$ ,  $\Delta_+$  and  $\Delta_-$  form a chiral multiplet, lead to the conclusion that  $\pi\Delta_\pm\Delta_\pm$  couplings (with like-charged  $\Delta$ s) are forbidden at tree-level. Quark-model arguments [19] suggest that the  $g_{\pi\Delta\Delta} = (4/5)g_{\pi NN}$ .

Lattice calculations for the nucleon axial charge  $g_A$  are available on a variety of ensembles and pion masses [26]. In addition, results on the axial  $N - \Delta$  transition from factor  $C_5^A$  [22] have been obtained on most of the ensembles used also in this work. We are therefore in position to perform a *combined chiral fit* using small scale expansion (SSE) within (HB $\chi$ PT) [27, 36, 37]. for  $g_A$ ,  $C_5^A(q^2)$  and the  $\Delta$  axial charge  $G_{\Delta\Delta}$  as functions of the pion mass  $m_\pi$ .

The one-loop SSE expression for  $C_5^A$  has been worked by Procura [37]. The expression for  $C_5^A(q^2)$  as a function of  $m_\pi$  is:

$$C_5^A = a_1 + a_2 m_\pi^2 + a_3 q^2 + \text{loop}_5(m_\pi), \quad (60)$$

where the loop integral contribution is:

$$\begin{aligned} \text{loop}_5(m_\pi) = & \frac{c_A}{15552 \pi^2 f_\pi^2} \left\{ \frac{1}{\Delta} \left[ \frac{5}{4} g_{\Delta\Delta}^2 (40\pi m_\pi^3 + 101\Delta m_\pi^2 + 24\Delta^3) + \frac{1170}{2} g_A g_{\Delta\Delta} m_\pi^2 \Delta \right. \right. \\ & - 12\Delta c_A^2 (162 m_\pi^2 - 83\Delta^2) - 27 g_A^2 (24\pi m_\pi^3 + 75\Delta m_\pi^2 - 40\Delta^3) \Big] \\ & + \frac{72}{\Delta} \sqrt{m_\pi^2 - \Delta^2} \left( m_\pi^2 c_A^2 - 28\Delta^2 c_A^2 + 18g_A^2 (m_\pi^2 - \Delta^2) \right) \arccos \left( -\frac{\Delta}{m_\pi} \right) \\ & - \frac{8}{\Delta} \sqrt{m_\pi^2 - \Delta^2} \left( 9 m_\pi^2 c_A^2 + 963 \Delta^2 c_A^2 + \frac{50}{4} g_{\Delta\Delta}^2 (m_\pi^2 - \Delta^2) \right) \arccos \left( \frac{\Delta}{m_\pi} \right) \\ & - \left[ 3 m_\pi^2 (900 c_A^2 - \frac{425}{4} g_{\Delta\Delta}^2 - \frac{450}{2} g_{\Delta\Delta} g_A + 81 g_A^2 + 648) \right. \\ & \left. \left. + 8\Delta^2 (-711 c_A^2 + \frac{50}{4} g_{\Delta\Delta}^2 + 162 g_A^2) \right] \ln \left( \frac{m_\pi}{\lambda} \right) \right\} \quad (61) \end{aligned}$$

Here  $\Delta = M_\Delta - M_N$ ,  $f_\pi = 92.4$  MeV,  $a_1, a_2, a_3$  are unknown parameters and  $\lambda$  is a cutoff scale set to  $\lambda = 1$  GeV.



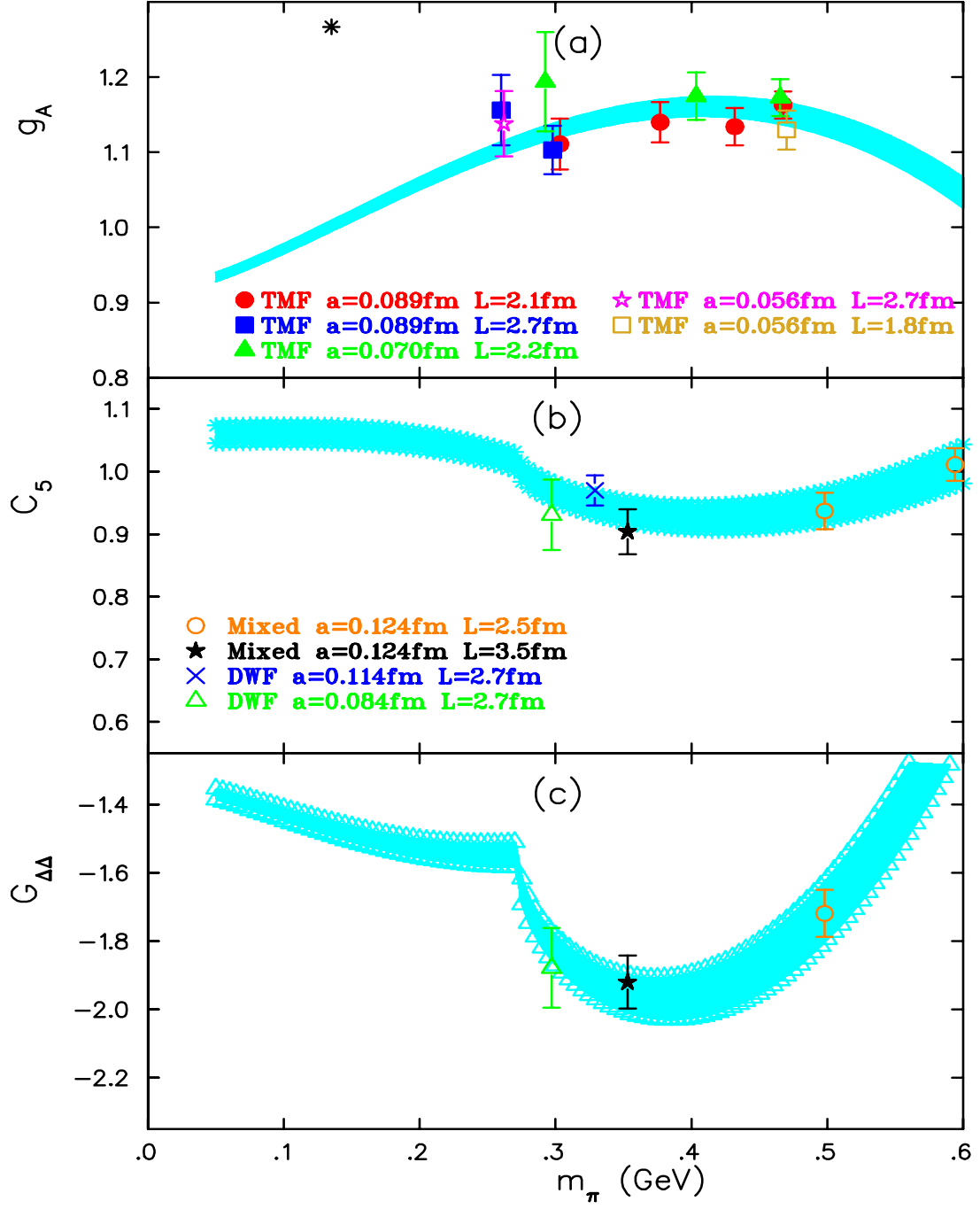


FIG. 18: Combined chiral fit: (a) Nucleon axial charge,  $g_A$ , fitted to lattice data obtained with  $N_f = 2$  twisted mass fermions (TMF) [26]. The physical value is shown by the asterisk; (filled circles:  $a=0.089$  fm,  $L=2.1$ , filled squares:  $a=0.089$  fm,  $L=2.8$  fm, filled triangles:  $a=0.070$  fm,  $L=2.2$  fm, open square:  $a=0.056$  fm,  $L=1.8$  fm, star:  $a=0.056$  fm,  $L=2.7$  fm); (b) Real part of axial N to  $\Delta$  transition coupling  $C_5^A(0)$  [22]; (open circles:  $a=0.124$  fm,  $L=2.5$  fm, filled square:  $a=0.124$  fm,  $L=3.5$  fm) and dynamical domain wall fermions (cross:  $a=0.114$  fm,  $L=2.7$  fm, open triangle:  $a=0.084$  fm,  $L=2.7$  fm); (c) Real part of  $\Delta$  axial charge  $G_{\Delta\Delta} = -3g_1(0)$ .

We use the SSE expression for the nucleon axial charge is presented in Ref. [38]

$$\begin{aligned}
g_A^{\text{SSE}}(m_\pi^2) = & g_A^0 - \frac{g_A^0{}^3 m_\pi^2}{16\pi^2 f_\pi^2} + 4 \left[ C^{\text{SSE}}(\lambda) + \frac{c_A^2}{4\pi^2 f_\pi^2} \left( \frac{155}{1944} g_{\Delta\Delta} - \frac{17}{36} g_A^0 \right) + \gamma^{\text{SSE}} \ln \frac{m_\pi}{\lambda} \right] m_\pi^2 \\
& + \frac{4c_A^2 g_A^0}{27\pi^2 f_\pi^2 \Delta} m_\pi^3 + \frac{8}{27\pi^2 f_\pi^2} c_A^2 g_A^0 m_\pi^2 \sqrt{1 - \frac{m_\pi^2}{\Delta^2}} \ln R \\
& + \frac{c_A^2 \Delta^2}{81\pi^2 f_\pi^2} \left( \frac{25}{2} g_{\Delta\Delta} - 57 g_A^0 \right) \left( \ln \frac{2\Delta}{m_\pi} - \sqrt{1 - \frac{m_\pi^2}{\Delta^2}} \ln R \right) + \mathcal{O}(\epsilon^4),
\end{aligned} \tag{62}$$

with

$$\begin{aligned}
\gamma^{\text{SSE}} &= \frac{-1}{16\pi^2 f_\pi^2} \left[ g_A^0 \left( \frac{1}{2} + g_A^0{}^2 \right) + \frac{2}{9} c_A^2 \left( g_A^0 - \frac{25}{18} g_{\Delta\Delta} \right) \right], \\
R &= \frac{\Delta}{m_\pi} + \sqrt{\frac{\Delta^2}{m_\pi^2} - 1}.
\end{aligned} \tag{63}$$

$g_A^0$  in the above expressions denotes the chiral limit value of the axial charge, i.e. corresponds to  $g_A$  in (61).

Finally, from Jiang and Tiburzi [27] we obtain the chiral expansion for the axial charge of the  $\Delta$ :

$$\begin{aligned}
G_{\Delta\Delta}(m_\pi^2) = & g_{\Delta\Delta} Z_\Delta - \frac{1}{(4\pi f_\pi)^2} \left[ g_{\Delta\Delta} \mathcal{L}(m_\pi, \mu) \left( 1 + \frac{121}{324} g_{\Delta\Delta}^2 \right) \right. \\
& + c_A^2 \left( \frac{8}{9} g_{\Delta\Delta} \mathcal{K}(m_\pi, -\Delta, \mu) - g_A \mathcal{J}(m_\pi, -\Delta, \mu) \right) \Big] \\
& + A m_\pi^2.
\end{aligned} \tag{64}$$

The  $\Delta$  field renormalization is

$$Z_\Delta = 1 - \frac{1}{32\pi^2 f_\pi^2} \left[ \frac{25}{18} g_{\Delta\Delta}^2 \mathcal{L}(m_\pi, \mu) + 2c_A^2 \mathcal{J}(m_\pi, -\Delta, \mu) \right]. \tag{65}$$

and the loop integrals from ([39]) evaluated at the scale  $\mu = 1$  GeV:

$$\begin{aligned}
\mathcal{L}(m, \mu) &= m^2 \log \left( \frac{m^2}{\mu^2} \right), \\
\mathcal{K}(m, \Delta, \mu) &= \left( m^2 - \frac{2}{3} \Delta^2 \right) \log \left( \frac{m^2}{\mu^2} \right) \\
&+ \frac{2}{3} \Delta \sqrt{\Delta^2 - m^2} \log \left( \frac{\Delta - \sqrt{\Delta^2 - m^2 + i\epsilon}}{\Delta + \sqrt{\Delta^2 - m^2 + i\epsilon}} \right) \\
&+ \frac{2}{3} \frac{m^2}{\Delta} \left( \pi m - \sqrt{\Delta^2 - m^2} \log \left( \frac{\Delta - \sqrt{\Delta^2 - m^2 + i\epsilon}}{\Delta + \sqrt{\Delta^2 - m^2 + i\epsilon}} \right) \right), \\
\mathcal{J}(m, \Delta, \mu) &= \left( m^2 - 2\Delta^2 \right) \log \left( \frac{m^2}{\mu^2} \right) \\
&+ 2\Delta \sqrt{\Delta^2 - m^2} \log \left( \frac{\Delta - \sqrt{\Delta^2 - m^2 + i\epsilon}}{\Delta + \sqrt{\Delta^2 - m^2 + i\epsilon}} \right),
\end{aligned} \tag{66}$$

From the available lattice data on  $C_5^A(q^2 = 0; m_\pi^2)$ ,  $g_A(m_\pi^2)$  and  $G_{\Delta\Delta}(m_\pi^2)$  we perform a simultaneous 7-parameter fit to expressions (60), (62) and (64) fitting the unknown constants  $a_1$ ,  $a_2$ ,  $A$ ,  $C^{\text{SSE}}$  as well as the common chiral couplings  $g_A$ ,  $c_A$  and  $g_{\Delta\Delta}$ . We note that  $C^{\text{SSE}}$  is independent of  $m_\pi$ ; at a fixed value of  $\lambda$  it can be fitted as a constant.

The lattice nucleon axial charge values  $g_A(m_\pi^2)$  are taken from twisted mass simulations [26]. Lattice values for the real part of the axial  $N - \Delta$  couplings  $C_5^A(0)$  are taken from [22] via a dipole extrapolation. The values of the real part of the axial charge of the  $\Delta$ ,  $G_{\Delta\Delta}(m_\pi^2)$  are related to the dominant axial form factor  $g_1$  at zero momentum transfer via  $G_{\Delta\Delta} = -3g_1(0)$ . For an additional lattice point to assist the fit we computed the zero-momentum  $g_1$  values (only) on the  $20^3 \times 64$  mixed-action ensemble with  $m_\pi = 498$  MeV. Values are provided in Table X.

In Figure 18 the combined fit is presented. The available lattice data for all three observables vary mildly in the pion mass regime considered.  $g_A$  remains underestimated with respect to the experimental value and the inclusion of  $C_5^A$  and  $G_{\Delta\Delta}$  into the SSE fit does not improve this systematically observed behavior. Strong chiral effects are expected at lighter pion mass values, especially below the  $\Delta$  decay threshold, as is evident from the 1-loop trend of  $C_5^A$  and  $G_{\Delta\Delta}$ .

## VI. CONCLUSIONS

A detailed study of the axial structure of the  $\Delta(1232)$  has been presented, complementing recent and ongoing studies of the axial structure of the nucleon as well as the axial  $N-$  to  $-\Delta$  transition. The matrix element of the  $\Delta$  state with the axial current has been parameterized via four Lorentz invariant form factors,  $g_1, g_3, h_1$  and  $h_3$ , and with two, denoted  $\tilde{g}$  and  $\tilde{h}$ , the pseudoscalar matrix element, generalizing the familiar nucleon axial structure. We detailed the lattice techniques required for the extraction of all six form factors for a complete  $q^2$ -dependent evaluation via specially designed three-point functions. In fact, the calculation is optimized such that only two sequential propagators are needed for the numerical evaluation of the optimal correlators. PCAC constrains strongly the nucleon matrix elements of the axial-vector and pseudoscalar currents as is manifestly evident by the phenomenological validity of the Goldberger-Treiman relation. Lattice QCD provides a check of this relation, which is a result of chiral symmetry breaking present in the QCD Lagrangian, confirming that the  $q^2$ -dependence of the axial and pseudoscalar form factors is in agreement with the PCAC predictions. Furthermore, the recent studies of the axial  $N-$  to  $-\Delta$  transition have shown that PCAC constrains strongly also the transition from factors and measurements of the dominant form factor  $C_5^A$  and  $G_{\pi N\Delta}$  provided a check of the non-diagonal GT relation. This work, examines extensions of similar relations for the  $\Delta$ . The main result of the current work is that PCAC plays a major role also in the relation between the  $\Delta$  matrix elements of the axial-vector and pseudoscalar currents, connecting the strength of the  $\pi - \Delta - \Delta$  vertex to the  $\Delta$  axial charge,  $G_{\Delta\Delta}$ . Actually, two independent pseudoscalar form factors,  $G_{\pi\Delta\Delta}$  and  $H_{\pi\Delta\Delta}$  are present and pion-pole dominance establishes relations among all six form factors. These predictions are qualitatively verified using results obtained in the quenched QCD study, which carries the smallest statistical noise. Results from two dynamical ensembles are consistent with these findings, albeit within large statistical errors. Having obtained an evaluation of  $g_A$  and  $C_5^A$  from previous studies and using the results of this work for  $G_{\Delta\Delta}$  on similar lattice ensembles, we performed a simultaneous chiral fit for all three utilizing one-loop chiral effective theory predictions in the SSE scheme which include a dynamical  $\Delta$  field. The seven-parameter fit does not drive the prediction near the experimentally known  $g_A$  value, and this is not surprising as it has become recently clear that the correct value of  $g_A$  is not reproduced even with pion masses very close to the physical one. A careful isolation of excited state effects [40, 41] at pion mass of about 400 MeV failed to reveal excited state contamination in the lattice extraction of  $g_A$ . Resolving such discrepancies is important for sharpening the predictive power of lattice QCD, which can yield phenomenologically important quantities not accessible experimentally. Fully chiral 2+1 domain wall flavour simulations are available now below the 300 MeV pion mass utilized in this work, and this leaves open the perspective for further investigations in the future which will elaborate on the relations studied in this work and on the values of the major couplings that dominate the low energy hadron interactions. However, as shown here, the gauge noise is large and noise-reduction techniques will be needed in order to extract useful results using ensembles with close to physical pion masses.

## ACKNOWLEDGEMENTS

We are grateful to Brian Tiburzi and K. S. Choi for helpful discussions. EBG was supported by Cyprus Research Promotion Foundation grant  $\Delta IE\Theta NH\Sigma/\Sigma TOXO\Sigma/0308/07$  and JWN in part by funds provided by the U.S. Department of Energy (DOE) under cooperative research agreement DE-FG02-94ER40818. Computer resources were provided by the National Energy Research Scientific Computing Center supported by the Office of Science of the DOE under Contract No. DE-AC02-05CH11231 and by the Jülich Supercomputing Center, awarded under the DEISA Extreme Computing Initiative, co-funded through the EU FP6 project RI-031513 and the FP7 project RI-222919. This research was in part supported by the Research Executive Agency of the European Union under Grant Agreement number PITN-GA-2009-238353 (ITN STRONGnet) and the Cyprus Research Promotion Foundation under contracts KY-ΓA/0310/02 and NEA YΠIOΔOMH/ΣTPATH/0308/31 (infrastructure project Cy-Tera co-funded by the European Regional Development Fund and the Republic of Cyprus through the Research Promotion Foundation).

### Appendix A: Multipole Form Factors

The axial vector transition between  $\Delta$  states can be parameterized via a multipole expansion. This is most naturally performed on the Breit frame, where  $\vec{p}_f = -\vec{p}_i = \vec{q}/2$ . Let us denote the matrix element as

$$\langle \Delta(\vec{q}/2, s_f) | \vec{A} \cdot \vec{\epsilon}_\lambda | \Delta(-\vec{q}/2, s_i) \rangle = M(s_f, s_i, \lambda). \quad (\text{A1})$$

Generically four different transitions will occur parameterized via

$$\begin{aligned} M\left(\frac{1}{2}, \frac{1}{2}, 0\right) &= L_1 + 3L_3 \\ M\left(\frac{3}{2}, \frac{3}{2}, 0\right) &= 3L_1 - L_3 \\ M\left(\frac{1}{2}, -\frac{1}{2}, 1\right) &= -2E_1 - \sqrt{6}E_3 \\ M\left(\frac{3}{2}, \frac{1}{2}, 1\right) &= -\sqrt{3}E_1 + \sqrt{2}E_3 \end{aligned} \quad (\text{A2})$$

with  $L_J, E_J$  the longitudinal and electric multipole amplitudes of rank  $J$ . The polarization vector  $\vec{\epsilon}_\lambda$  has components  $\vec{\epsilon}_+ = -(\hat{x} + i\hat{y})/\sqrt{2}$ ,  $\vec{\epsilon}_- = -\vec{\epsilon}_+^*$ ,  $\vec{\epsilon}_0 = \hat{z}$ .

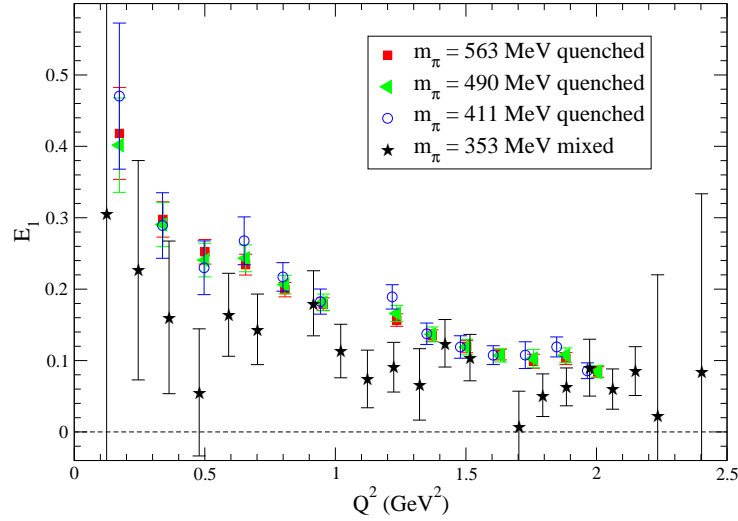
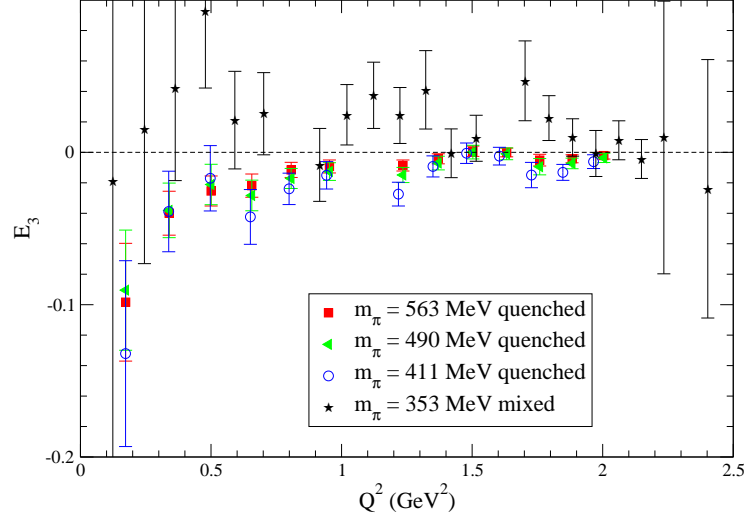
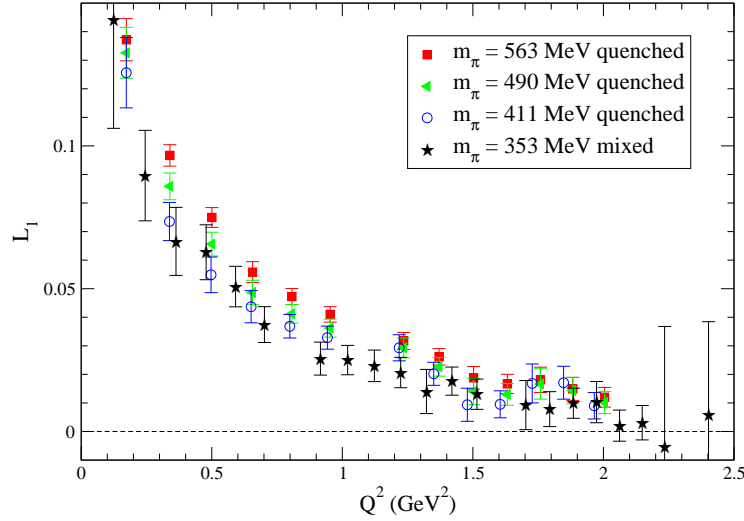


FIG. 19: Lattice results for the  $E_1$  multipole axial form-factor.

We can relate the form factors  $g_1, g_3, h_1$  and  $h_3$  to the multipole form factors  $E_1, E_3, L_1$  and  $L_3$ , which have physical relevance in the multipole expansion.

$$\begin{aligned} g_1 &= \frac{3}{\sqrt{2}}E_1 + \sqrt{3}E_3 \\ \tau(1+\tau)h_1 &= -3\sqrt{2}\tau E_1 + \frac{5+4\tau}{2}\sqrt{3}E_3 \\ (g_1 - \tau g_3) &= \sqrt{1+\tau}(3L_1 - L_3) \\ \tau(1+\tau)(h_1 - \tau h_3) &= \sqrt{1+\tau}(-6\tau L_1 + (5+2\tau)L_3) \end{aligned} \quad (\text{A3})$$

from which the reverse relations can be verified:

FIG. 20: Lattice results for the  $E_3$  multipole axial form-factor.FIG. 21: Lattice results for the  $L_1$  multipole axial form-factor.

$$E_1 = \frac{\sqrt{2}g_1}{3} - \frac{2\sqrt{2}\tau(2g_1 + h_1(1 + \tau))}{3(5 + 8\tau)} \quad (\text{A4})$$

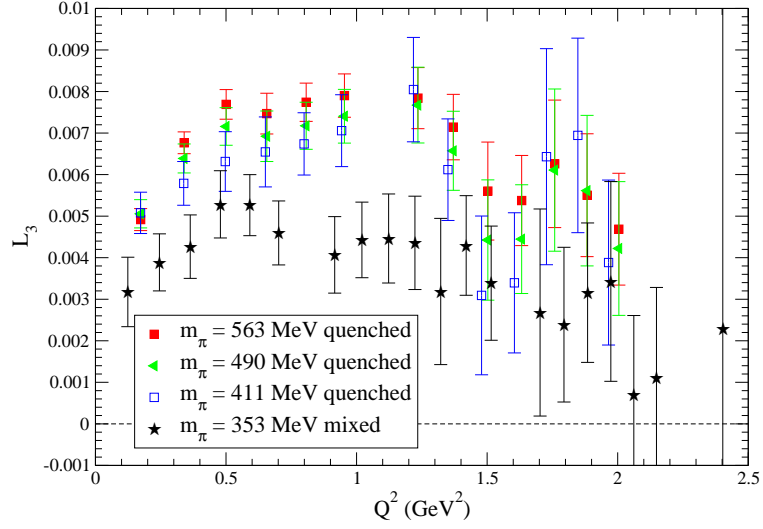
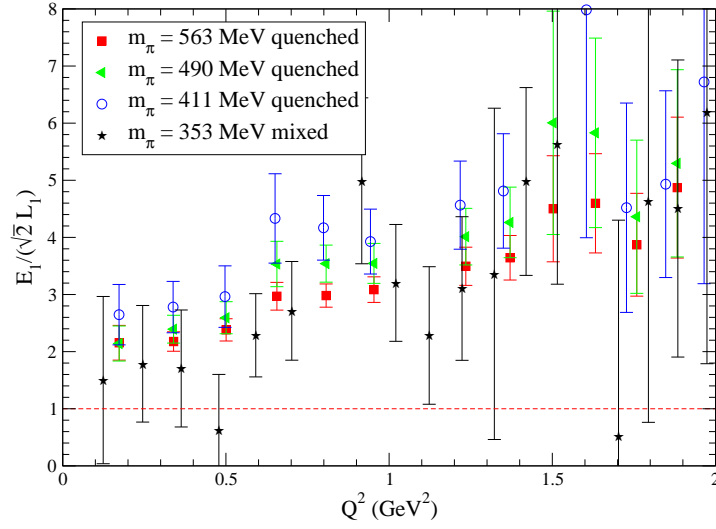
$$E_3 = \frac{2\tau(2g_1 + h_1(1 + \tau))}{\sqrt{3}(5 + 8\tau)} \quad (\text{A5})$$

$$L_1 = \frac{(5 + 2\tau)(g_1 - \tau g_3) + \tau(1 + \tau)(h_1 - \tau h_3)}{15\sqrt{1 + \tau}} \quad (\text{A6})$$

$$L_3 = \tau \frac{2(g_1 - \tau g_3) + (1 + \tau)(h_1 - \tau h_3)}{5\sqrt{1 + \tau}}. \quad (\text{A7})$$

Utilizing the above relations, we present results on the four multipole axial form-factors,  $E_1$ ,  $E_3$ ,  $L_1$  and  $L_3$ , in Figures 19, 20, 21 and 22, respectively.

In the low momentum transfer limit,  $\tau \sim \mathcal{O}(\bar{q}^2/M_\Delta^2) \ll 1$  and from relations (A5, A7) we deduce that  $E_3, L_3 \ll 1$ . On the other hand,  $E_1$  and  $L_1$  remain finite, as from relation (A4)  $E_1 \sim \sqrt{2}g_1/3$  and from (A6)  $L_1 \sim g_1/3$ . Thus at

FIG. 22: Lattice results for the  $L_3$  multipole axial form-factor.FIG. 23: Lattice results for the ratio of the  $E_1$  to  $\sqrt{2}L_1$  multipole axial form-factors for the quenched ensembles.

the low momentum transfer limit we expect that  $E_1 = \sqrt{2}L_1 + \mathcal{O}(\vec{q}^2)$ .

We test these predictions explicitly in Figure 23 where the ratio  $E_1/\sqrt{2}L_1$  is plotted. We observe a behavior consistent with a constant in the low energy ( $< 0.5\text{GeV}^2$ ) regime although the numeric value of the constant is largely overestimated by the quenched lattice data. In addition, this constancy is in accordance to the pion-pole dependence of both  $E_1$  and  $L_1$  which is evident from the quenched lattice data plotted in Figs. (19) and (21). Despite the large statistical uncertainties,  $E_3$  and  $L_3$  are consistent with small values at small momentum transfers.

## Appendix B: Trace algebra for 3-point correlators

### 1. Axial current correlator

We define Type I as

$$\Pi_{\mu}^{IA}(q) \equiv \sum_{i=1}^3 \sum_{\sigma, \tau=1}^3 \delta_{\sigma\tau} \text{tr} [\Gamma^i \Lambda_{\sigma\sigma'}(p_f) \mathcal{O}_{\sigma'\mu\tau'}^A \Lambda_{\tau'\tau}(p_i)] . \quad (\text{B1})$$

After evaluating the Dirac traces we find two distinct cases,  $\mu = 4$  and  $\mu = 1, 2, 3$ . The kinematical frame is set to  $\vec{p}_f = 0$  and  $\vec{p}_i = -\vec{q}$ . We note by  $E = (\vec{p}^2 + M_{\Delta}^2)^{1/2}$ .

For  $\mu = 4$  we find

$$\begin{aligned} \Pi_{\mu=4}^{IA}(q) = \frac{-1}{36M_{\Delta}^3} & \left[ 2(2E^2 - 2EM_{\Delta} + 5M_{\Delta}^2)(g_1 - \tau g_3) \right. \\ & \left. - \tau(2E - M_{\Delta})(E + M_{\Delta})(h_1 - \tau h_3) \right] (p_1 + p_2 + p_3) , \end{aligned} \quad (\text{B2})$$

using

$$\tau \equiv \frac{(E - M_{\Delta})}{2M_{\Delta}} = \frac{Q^2}{(2M_{\Delta})^2} . \quad (\text{B3})$$

For  $\mu = i$  we find

$$\begin{aligned} \Pi_{\mu=i}^{IA}(q) = \frac{i(E + M_{\Delta})}{18M_{\Delta}^3} & \left[ (2E^2 + 3M_{\Delta}^2)g_1 - \tau E(E + M_{\Delta})h_1 \right] \\ - \frac{i}{72M_{\Delta}^4} & \left[ 8M_{\Delta}^2 g_1 + 2(2E^2 - 2EM_{\Delta} + 5M_{\Delta}^2)g_3 \right. \\ & \left. - M_{\Delta}(E + M_{\Delta})h_1 - \tau(E + M_{\Delta})(2E - M_{\Delta})h_3 \right] p_i (p_1 + p_2 + p_3) . \end{aligned} \quad (\text{B4})$$

We define Type II as:

$$\Pi_{\mu}^{IIA}(q) \equiv \sum_{\sigma, \tau=1}^3 T_{\sigma\tau} \text{tr} [\Gamma^4 \Lambda_{\sigma\sigma'}(p_f) \mathcal{O}_{\sigma'\mu\tau'}^A \Lambda_{\tau'\tau}(p_i)] \quad (\text{B5})$$

$$T_{\sigma\tau} = \begin{bmatrix} 0 & 1 & -1 \\ -1 & 0 & 1 \\ 1 & -1 & 0 \end{bmatrix} . \quad (\text{B6})$$

For  $\mu = 4$  we find

$$\begin{aligned} \Pi_{\mu=4}^{IIA}(q) = \frac{i}{18M_{\Delta}^2} & \left[ (E + 4M_{\Delta})(g_1 - \tau g_3) \right. \\ & \left. - \frac{\tau}{2}(E + M_{\Delta})(h_1 - \tau h_3) \right] (p_1 + p_2 + p_3) . \end{aligned} \quad (\text{B7})$$

For  $\mu = i$  we find

$$\begin{aligned} \Pi_{\mu=i}^{IIA}(q) = \frac{(E + M_{\Delta})^2}{36M_{\Delta}^3} & \left[ (2E + 3M_{\Delta})g_1 - \tau(E + M_{\Delta})h_1 \right] \\ - \frac{1}{36M_{\Delta}^3} & \left[ (2E + 5M_{\Delta})g_1 + (E + 4M_{\Delta})g_3 \right. \\ & \left. - \frac{E}{2m}(E + M_{\Delta})h_1 - \frac{\tau}{2}(E + M_{\Delta})h_3 \right] p_i (p_1 + p_2 + p_3) . \end{aligned} \quad (\text{B8})$$



## 2. Pseudoscalar density correlator

In a similar way we evaluate the trace algebra for the pseudoscalar vertices. The index summation types are defined in the same way as in the axial case. Pseudoscalar Type I is

$$\Pi_{\text{PS}}^I(q) \equiv \sum_{i=1}^3 \sum_{\sigma, \tau=1}^3 \delta_{\sigma\tau} \text{tr} [\Gamma^i \Lambda_{\sigma\sigma'}(p_f) \mathcal{O}_{\sigma'\tau'}^{\text{PS}} \Lambda_{\tau'\tau}(p_i)] . \quad (\text{B9})$$

After the trace evaluation we find:

$$\begin{aligned} \Pi_{\text{PS}}^I(q) = & \frac{-1}{18M_\Delta^3} \left[ \tilde{g} (2E^2 - 2EM_\Delta + 5M_\Delta^2) \right. \\ & \left. - \tilde{h} \frac{\tau}{2} (2E - M_\Delta) (E + M_\Delta) \right] (p_1 + p_2 + p_3) \end{aligned} \quad (\text{B10})$$

Pseudoscalar Type II is

$$\Pi_{\text{PS}}^{II}(q) \equiv \sum_{\sigma, \tau=1}^3 T_{\sigma\tau} \text{tr} [\Gamma^4 \Lambda_{\sigma\sigma'}(p_f) \mathcal{O}_{\sigma'\tau'}^{\text{PS}} \Lambda_{\tau'\tau}(p_i)] , \quad (\text{B11})$$

giving us

$$\Pi_{\text{PS}}^{II}(q) = \frac{i}{18M_\Delta^2} \left[ (E + 4M_\Delta) \tilde{g} - \frac{\tau}{2} (E + M_\Delta) \tilde{h} \right] (p_1 + p_2 + p_3) \quad (\text{B12})$$

after we evaluate the trace.

## Appendix C: Form Factor results

- 
- [1] K. Jansen (2008), 0810.5634.
  - [2] S. Durr et al., Science **322**, 1224 (2008).
  - [3] S. Aoki et al. (PACS-CS), Phys. Rev. D **79**, 034503 (2009), 0807.1661.
  - [4] S. Durr, Z. Fodor, C. Hoelbling, S. Katz, S. Krieg, et al., JHEP **1108**, 148 (2011), 1011.2711.
  - [5] C. Alexandrou et al. (ETM Collaboration), Phys.Rev. **D80**, 114503 (2009), 0910.2419.
  - [6] S. Aoki et al. (PACS-CS Collaboration), Phys.Rev. **D81**, 074503 (2010), 0911.2561.
  - [7] S. Beane et al. (NPLQCD Collaboration), Phys.Rev. **D85**, 034505 (2012), 1107.5023.
  - [8] J. J. Dudek, R. G. Edwards, and C. E. Thomas, Phys.Rev. **D86**, 034031 (2012), 1203.6041.
  - [9] X. Feng, K. Jansen, and D. B. Renner, Phys.Lett. **B684**, 268 (2010), 0909.3255.
  - [10] T. Yamazaki et al. (CP-PACS Collaboration), Phys.Rev. **D70**, 074513 (2004), hep-lat/0402025.
  - [11] M. Kotulla, J. Ahrens, J. Annand, R. Beck, G. Caselotti, et al., Phys.Rev.Lett. **89**, 272001 (2002), nucl-ex/0210040.
  - [12] G. Lopez Castro and A. Mariano, Phys.Lett. **B517**, 339 (2001), nucl-th/0006031.
  - [13] V. Bernard, T. R. Hemmert, and U.-G. Meissner, Phys.Lett. **B622**, 141 (2005), hep-lat/0503022.
  - [14] T. R. Hemmert, B. R. Holstein, and J. Kambor, J.Phys. **G24**, 1831 (1998), hep-ph/9712496.
  - [15] E. E. Jenkins and A. V. Manohar, Phys.Lett. **B259**, 353 (1991).
  - [16] N. Fettes and U. G. Meissner, Nucl.Phys. **A679**, 629 (2001), hep-ph/0006299.
  - [17] V. Bernard, Prog.Part.Nucl.Phys. **60**, 82 (2008), 0706.0312.
  - [18] R. F. Dashen, E. E. Jenkins, and A. V. Manohar, Phys.Rev. **D49**, 4713 (1994), hep-ph/9310379.
  - [19] G. Brown and W. Weise, Phys.Rept. **22**, 279 (1975).
  - [20] K.-S. Choi, W. Plessas, and R. Wagenbrunn, Phys.Rev. **D82**, 014007 (2010), 1005.0337.
  - [21] C. Alexandrou, G. Koutsou, T. Leontiou, J. W. Negele, and A. Tsapalis, Phys.Rev. **D76**, 094511 (2007), 0912.0394.
  - [22] C. Alexandrou, G. Koutsou, J. Negele, Y. Proestos, and A. Tsapalis, Phys.Rev. **D83**, 014501 (2011), 1011.3233.
  - [23] C. Alexandrou, T. Korzec, G. Koutsou, C. Lorce, J. W. Negele, et al., Nucl.Phys. **A825**, 115 (2009), 0901.3457.
  - [24] C. Alexandrou, C. Papanicolas, and M. Vanderhaeghen (2012), 1201.4511.
  - [25] C. Alexandrou, E. B. Gregory, T. Korzec, G. Koutsou, J. W. Negele, et al., Phys.Rev.Lett. **107**, 141601 (2011), 1106.6000.

- [26] C. Alexandrou et al. (ETM Collaboration), Phys.Rev. **D83**, 045010 (2011), 1012.0857.
- [27] F.-J. Jiang and B. C. Tiburzi, Phys.Rev. **D78**, 017504 (2008), 0803.3316.
- [28] [Http://www.nikhef.nl/~form](http://www.nikhef.nl/~form).
- [29] A. Tsapalis, Nucl.Phys.Proc.Suppl. **153**, 320 (2006).
- [30] C. W. Bernard, T. Burch, K. Orginos, D. Toussaint, T. A. DeGrand, et al., Phys.Rev. **D64**, 054506 (2001), hep-lat/0104002.
- [31] Y. Aoki et al. (RBC Collaboration, UKQCD Collaboration), Phys.Rev. **D83**, 074508 (2011), 1011.0892.
- [32] V. Belyaev, B. Y. Blok, and Y. Kogan, Sov.J.Nucl.Phys. **41**, 280 (1985).
- [33] S.-L. Zhu, Phys.Rev. **C63**, 018201 (2001), nucl-th/0009062.
- [34] G. Erkol, <http://irs.ub.rug.nl/ppn/297396218>.
- [35] D. Jido, T. Hatsuda, and T. Kunihiro, Phys.Rev.Lett. **84**, 3252 (2000), hep-ph/9910375.
- [36] T. R. Hemmert, M. Procura, and W. Weise, Phys.Rev. **D68**, 075009 (2003), hep-lat/0303002.
- [37] M. Procura, Phys.Rev. **D78**, 094021 (2008), 0803.4291.
- [38] M. Procura, B. Musch, T. Hemmert, and W. Weise, Phys.Rev. **D75**, 014503 (2007), hep-lat/0610105.
- [39] F.-J. Jiang and B. C. Tiburzi, Phys.Rev. **D77**, 094506 (2008), 0801.2535.
- [40] S. Dinter, C. Alexandrou, M. Constantinou, V. Drach, K. Jansen, et al., Phys.Lett. **B704**, 89 (2011), 1108.1076.
- [41] C. Alexandrou, M. Constantinou, S. Dinter, V. Drach, K. Jansen, et al., PoS **LATTICE2011**, 150 (2011), 1112.2931.

	$Q^2$ (GeV <sup>2</sup> )	Axial				Pseudoscalar	
		$g_1$	$g_3$	$h_1$	$h_3$	$\tilde{g}$	$\tilde{h}$
$m_\pi = 563(4)$ MeV	0.000000	0.5887(98)	—	—	—	—	—
	0.1730731	0.717(70)	15.3(3.2)	22.9(8.6)	740(380)	9.58(43)	46(89)
	0.3396915	0.562(27)	6.96(65)	5.6(1.7)	103(37)	7.14(19)	46(17)
	0.5005274	0.491(20)	4.63(38)	2.89(79)	38(16)	5.42(18)	17.4(8.5)
	0.6561444	0.459(19)	3.86(25)	2.15(48)	24.7(7.4)	4.13(17)	10.3(5.5)
	0.8070197	0.403(14)	2.81(15)	1.30(26)	11.7(3.1)	3.44(14)	10.1(2.9)
	0.9535618	0.364(14)	2.20(11)	1.04(19)	7.7(2.1)	2.91(13)	8.6(1.9)
	1.235014	0.318(14)	1.57(10)	0.84(14)	4.4(1.1)	2.12(14)	5.5(1.3)
	1.370502	0.279(14)	1.272(81)	0.61(11)	2.91(87)	1.73(12)	4.21(92)
	1.502826	0.255(14)	1.151(89)	0.41(11)	2.38(79)	1.35(13)	2.34(90)
	1.632198	0.230(13)	0.959(68)	0.388(84)	1.97(54)	1.17(11)	2.08(69)
	1.758807	0.201(17)	0.730(86)	0.45(11)	1.84(64)	1.05(14)	1.95(72)
	1.882824	0.211(16)	0.769(76)	0.439(69)	1.69(41)	0.92(13)	1.52(57)
	2.004400	0.175(14)	0.604(65)	0.327(58)	1.24(31)	0.73(10)	1.18(43)
	2.240774	0.124(22)	0.43(11)	3.249(98)	4.66(48)	0.40(16)	0.48(60)

TABLE XI: Delta form factors from quenched Wilson fermions.

	$Q^2$ (GeV <sup>2</sup> )	Axial				Pseudoscalar	
		$g_1$	$g_3$	$h_1$	$h_3$	$\tilde{g}$	$\tilde{h}$
$m_\pi = 490(4)$ MeV	0.000000	0.578(13)	—	—	—	—	—
	0.1728690	0.695(72)	14.0(2.9)	20.0(8.3)	390(330)	10.85(62)	120(130)
	0.3389351	0.550(36)	7.03(78)	5.1(2.0)	97(41)	7.69(27)	59(23)
	0.4989433	0.474(28)	4.52(45)	2.4(1.1)	33(17)	5.78(23)	26(11)
	0.6535119	0.467(23)	3.99(31)	2.45(60)	26.8(9.0)	4.23(22)	10.3(6.8)
	0.8031605	0.408(17)	2.88(18)	1.53(33)	13.1(3.6)	3.54(17)	11.6(3.3)
	0.9483310	0.363(16)	2.18(14)	1.14(25)	8.1(2.4)	2.98(16)	8.9(2.3)
	1.226705	0.326(17)	1.58(12)	1.02(18)	5.1(1.4)	2.21(17)	5.9(1.5)
	1.360524	0.278(16)	1.253(95)	0.67(14)	3.2(1.0)	1.75(14)	4.1(1.1)
	1.491113	0.252(17)	1.14(10)	0.42(13)	2.59(93)	1.30(14)	2.0(1.1)
	1.618694	0.226(15)	0.935(78)	0.40(11)	2.02(63)	1.15(13)	2.01(82)
	1.743467	0.202(20)	0.71(10)	0.54(14)	2.17(77)	1.02(16)	1.50(89)
	1.865609	0.216(19)	0.751(87)	0.501(87)	1.74(48)	0.99(15)	1.79(70)
	1.985279	0.173(16)	0.580(71)	0.348(73)	1.25(36)	0.73(12)	1.10(50)
	2.217769	0.110(24)	0.41(12)	-0.09(13)	-0.02(58)	0.31(18)	0.21(72)

TABLE XII: Delta form factors from quenched Wilson fermions.

	$Q^2$ (GeV <sup>2</sup> )	Axial				Pseudoscalar	
		$g_1$	$g_3$	$h_1$	$h_3$	$\tilde{g}$	$\tilde{h}$
$m_\pi = 411(4)$ MeV	0.000000	0.571(18)	—	—	—	—	—
	0.1726468	0.77(11)	17.4(4.5)	27(12)	560(490)	13.1(1.1)	290(230)
	0.3381149	0.546(52)	7.4(1.1)	4.9(2.7)	102(61)	8.27(45)	59(40)
	0.4972318	0.458(44)	4.53(66)	2.0(1.6)	33(24)	6.17(36)	27(18)
	0.6506769	0.495(41)	4.28(51)	3.2(1.0)	32(15)	4.48(31)	15.4(9.8)
	0.7990168	0.419(26)	2.96(25)	1.81(49)	13.4(5.2)	3.73(23)	14.4(4.4)
	0.9427295	0.361(23)	2.14(19)	1.21(37)	7.5(3.4)	3.16(22)	11.2(3.2)
	1.217848	0.354(25)	1.68(16)	1.42(26)	6.4(2.0)	2.41(25)	7.5(2.3)
	1.349909	0.276(22)	1.23(12)	0.72(21)	3.4(1.4)	1.78(18)	4.4(1.4)
	1.478675	0.251(24)	1.16(13)	0.44(19)	3.1(1.3)	1.23(18)	1.8(1.5)
	1.604379	0.224(20)	0.93(10)	0.43(16)	2.26(87)	1.15(16)	2.4(1.1)
	1.727230	0.203(28)	0.68(13)	0.65(21)	2.5(1.1)	0.96(21)	1.0(1.3)
	1.847415	0.230(24)	0.75(11)	0.63(13)	1.87(64)	1.16(20)	2.9(1.0)
	1.965099	0.171(18)	0.565(85)	0.39(10)	1.32(47)	0.73(15)	1.13(68)
	2.193551	9.100(30)	0.37(14)	-0.18(19)	8.70(83)	0.16(21)	-0.2(1.1)

TABLE XIII: Delta form factors from quenched Wilson fermions. Results for  $h_1$  and  $h_3$  are plagued by statistical noise.

	$Q^2$ (GeV <sup>2</sup> )	Axial				Pseudoscalar	
		$g_1$	$g_3$	$h_1$	$h_3$	$\tilde{g}$	$\tilde{h}$
$m_\pi = 353(4)$ MeV	0.000000	0.640(26)	—	—	—	—	—
	0.1240682	0.62(39)	15(26)	8(74)	-100(4500)	14.4(4.8)	230(1800)
	0.2450231	0.51(17)	9.8(6.0)	-2(16)	120(540)	11.7(1.8)	440(320)
	0.3630880	0.41(12)	6.0(3.1)	-4.4(7.7)	-25(200)	9.1(1.2)	260(140)
	0.4784607	0.28(10)	1.9(2.1)	-8.1(4.9)	-160(104)	7.0(1.1)	87(83)
	0.5913172	0.385(69)	4.0(1.1)	-0.9(2.5)	-7(40)	5.88(67)	85(37)
	0.7018154	0.349(60)	3.42(78)	-1.0(1.9)	2(25)	5.41(61)	87(27)
	0.9162911	0.368(57)	3.22(60)	1.1(1.3)	21(15)	3.46(56)	29(17)
	1.020513	0.283(47)	2.07(43)	-0.6(1.0)	-0.3(9.3)	3.43(51)	35(12)
	1.122869	0.222(50)	1.39(43)	-1.15(98)	-9.6(8.5)	2.22(52)	17(11)
	1.223456	0.234(45)	1.43(36)	-0.50(77)	-3.2(6.3)	2.26(48)	13.3(8.5)
	1.322363	0.212(66)	1.31(51)	-1.1(1.0)	-5.6(8.1)	2.34(77)	18(13)
	1.419670	0.262(46)	1.50(31)	0.48(60)	2.5(4.2)	1.70(50)	7.0(7.1)
	1.515454	0.237(48)	1.32(30)	0.12(53)	2.0(3.6)	2.08(54)	12.3(6.3)
	1.702723	9.586(67)	0.41(38)	-1.15(83)	-6.4(4.8)	1.25(99)	14(11)
	1.794332	0.148(44)	0.70(24)	-0.35(44)	-1.8(2.5)	1.07(56)	8.4(5.2)
	1.884666	0.151(39)	0.65(20)	0.00(66)	-0.3(2.0)	0.90(48)	3.1(4.0)
	1.973777	0.190(66)	0.82(32)	0.34(44)	1.3(2.3)	0.65(67)	-6.1(5.8)
	2.061714	0.141(42)	0.66(20)	0.05(35)	0.5(1.8)	0.37(52)	5.4(4.0)
	2.148521	0.173(56)	0.77(26)	0.38(35)	2.1(1.7)	1.07(59)	4.3(4.1)
	2.234241	0.06(31)	0.4(1.6)	-0.1(2.6)	0.0(11.0)	-0.5(3.5)	-5(32)
	2.402577	0.14(39)	0.5(1.5)	0.7(2.3)	2.5(9.2)	1.0(3.4)	2(18)

TABLE XIV: Delta form factors from mixed-action fermions.

	$Q^2$ (GeV <sup>2</sup> )	Axial				Pseudoscalar	
		$g_1$	$g_3$	$h_1$	$h_3$	$\tilde{g}$	$\tilde{h}$
$m_\pi = 297(5)$ MeV	0.0	0.604(38)	—	—	—	—	—
	0.2060893	0.08(45)	-5.6(18.0)	-44(45)	-1500(2000)	9.4(9.3)	-1100(1800)
	0.4030337	0.66(20)	9.3(4.3)	11(10)	130(240)	6.6(3.0)	-300(280)
	0.5919523	0.79(19)	10.3(2.9)	13(6)	210(110)	4.5(2.4)	-82(140)
	0.7737530	0.41(20)	3.5(2.3)	2.2(5.2)	8(65)	7.2(2.2)	125(90)
	0.9491845	0.21(12)	0.6(1.7)	-1.0(2.5)	-34(25)	4.5(1.3)	42(39)
	1.118873	0.51(14)	3.9(1.1)	4.8(2.2)	45(19)	1.3(1.4)	-20(32)
	1.443061	0.47(21)	2.3(1.3)	4.3(2.6)	21(17)	3.2(1.9)	27(30)
	1.598405	0.31(14)	1.25(76)	2.1(1.6)	4.7(8.8)	0.1(1.2)	-1(16)
	1.749719	0.14(13)	0.91(69)	0.0(1.3)	2.2(7.2)	0.2(1.4)	-12(16)
	1.897302	-0.09(29)	-0.3(1.4)	-2.2(3.2)	-11(16)	-4.6(4.6)	-62(57)
	2.041417	-0.03(33)	0.1(1.6)	-0.4(2.9)	3(14)	0.2(3.1)	6(33)
	2.182297	0.17(23)	0.51(91)	0.8(1.8)	4.6(7.7)	2.8(2.7)	9(18)
	2.320150	-0.06(14)	-0.41(57)	-0.7(1.1)	-3.6(4.4)	0.4(1.4)	2(11)

TABLE XV: Delta form factors from Domain-Wall fermions.